Consistency of Ice Cloud Models in Forward Retrieval and Radiative Forcing Assessment

PI: Ping Yang

Dept. of Atmospheric Sciences/ Dept. of Physics & Astronomy, Texas A&M University, College Station, TX

Non-funded collaborator: Norman Loeb

NASA Langley Research Center, Hampton, VA

Contributions to this presentation: M. Saito, S. Hioki, and C. P. Kuo

Cirrus (Ci)

Cirrostratus (Cs)

Cirrocumulus (Cu)

Altocumulus (Ac)

Altostratus (As)

Stratocumulus (Sc)

Stratus (St)

Cumulus (Cu, Fairweather)

Taken from http://www.clouds-online.com. Copyright information: http://www.clouds-online.com/imprint.htm except for Cirrus (taken from http://www.c-f-r.dk/images/Artikelbilleder_540_200px/cirrus_over_warsaw_june_26_2005.jpg) & Altostratus (http://cimss.ssec.wisc.edu/satmet/gallery/images/altostratus.jpg).

Ice Cloud Fraction based on MODIS Collection 6 data

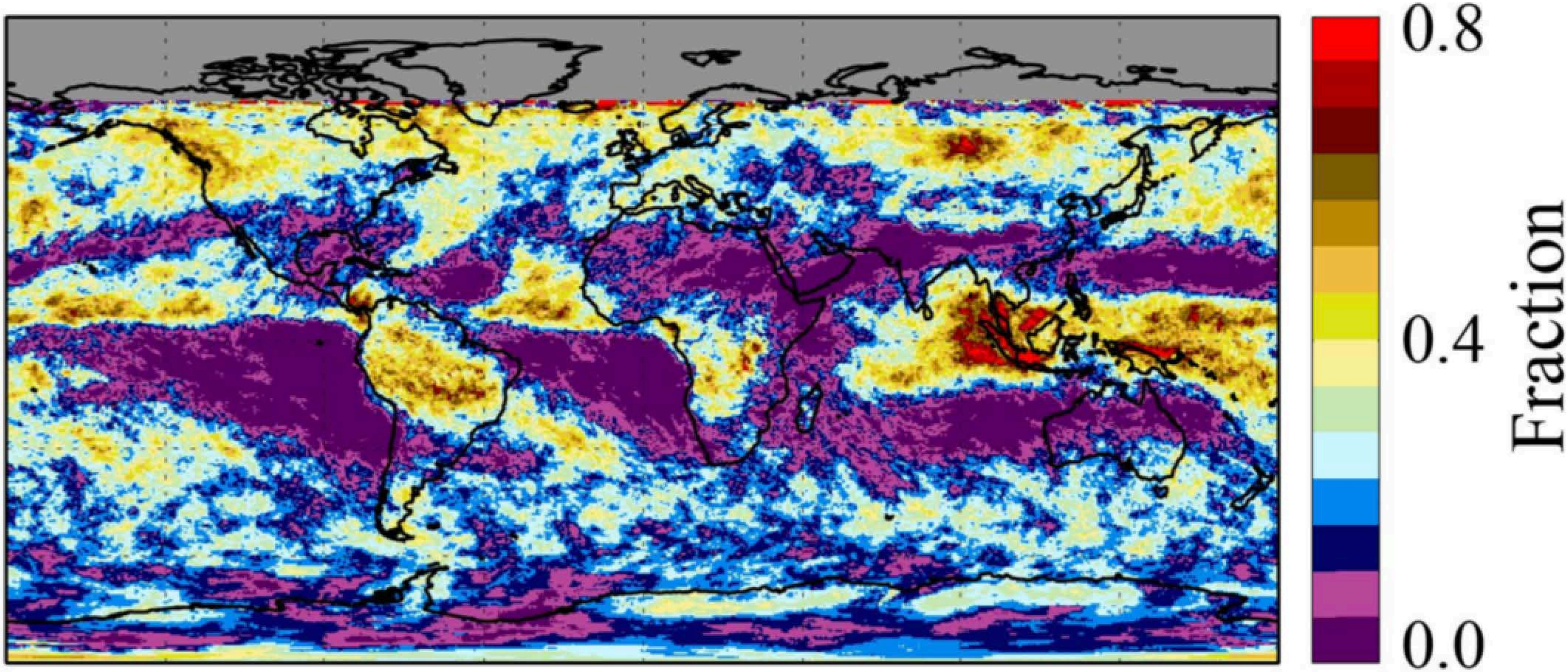

November 2012 Aqua MODIS monthly cloud fraction (Platnick et al. 2017)

Global Ice Cloud Coverage

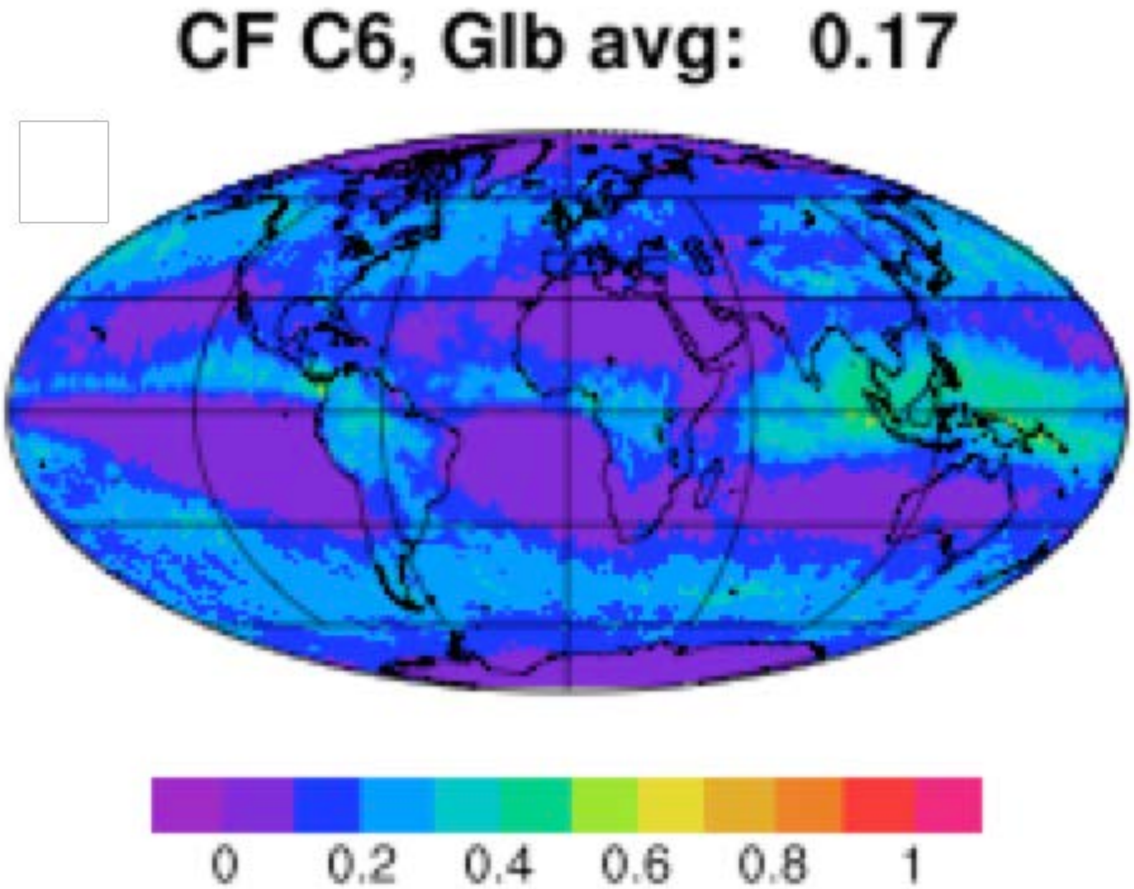

Ice cloud coverage (Yi et al. 2017) based on one year (2012) of level-2 MODIS Collection 6 cloud products (Platnick, Meyer et al. 2016)

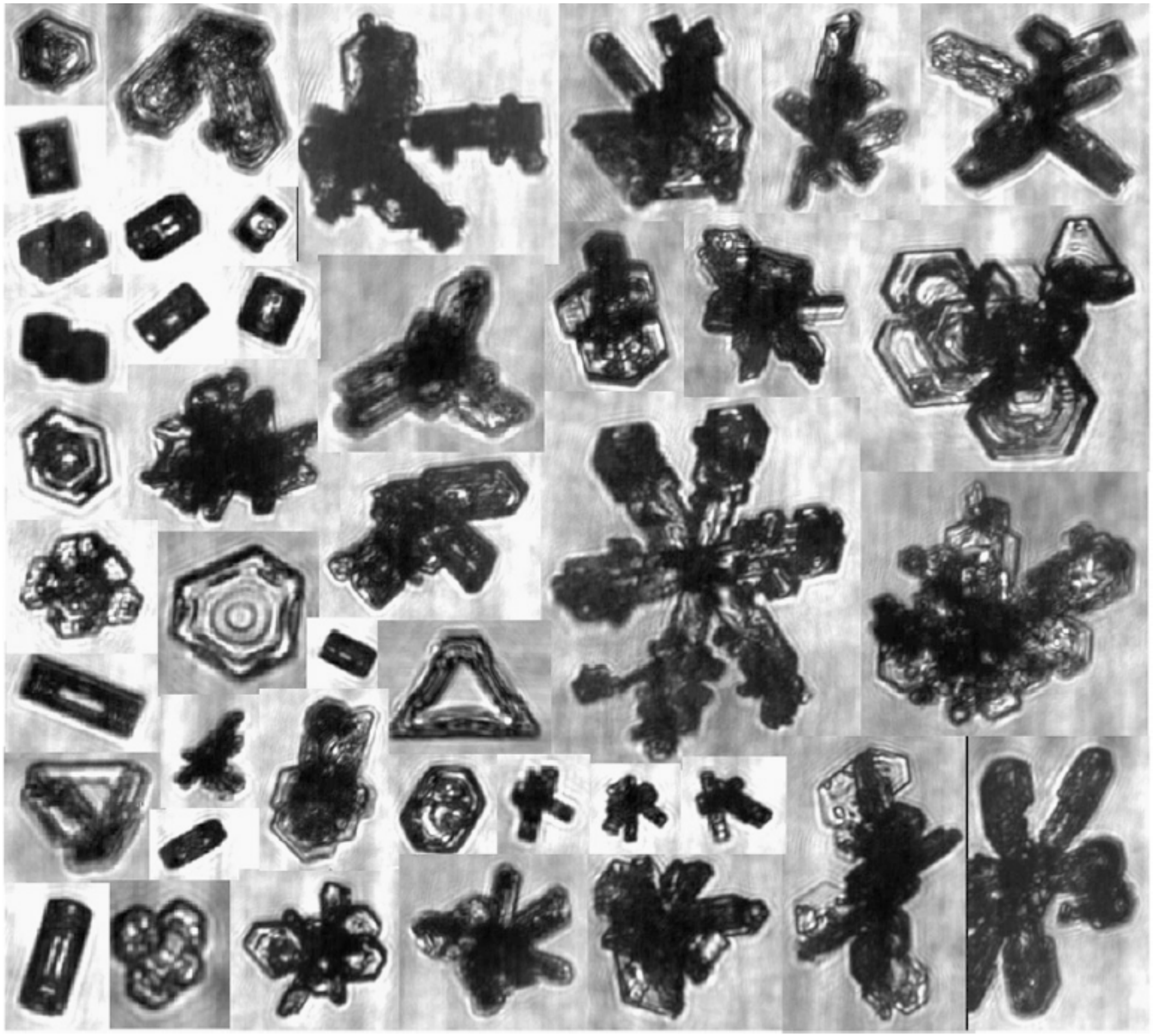

Bailey, M. P., and J. Hallett, 2009: A comprehensive habit diagram for atmospheric ice crystals: Confirmation from the laboratory, AIRS II, and other field studies, J. Atmos. Sci., 66(9), 2888-2899, doi=10.1175/2009JAS2883.1.

*Stephens, G. L., S.-C. Tsay, P. W. Stackhouse Jr., and P. J. Flatau, 1990: The relevance of the microphysical and radiative properties of cirrus clouds to climate and climatic feedback. J. Atmos. Sci., **47**, 1742–1754.*

- "The asymmetry parameter had to be adjusted from the broadband **Mie value** of g=0.87 for the size distribution chosen to a lower value of g=0.7 in order to bring the observations and theory into broad agreement."
- "Cirrus clouds characterized by g=0.87 warmed approximately twice as much as cirrus clouds modeled with g=0.7."

Retrieved optical thickness based on MODIS observations

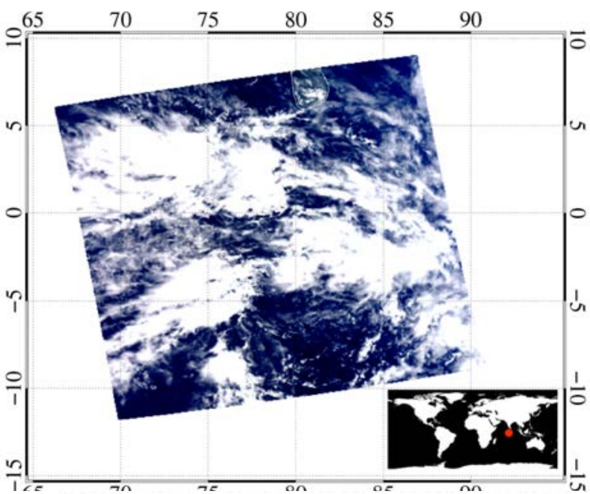

Hexagonal Ice Crystals

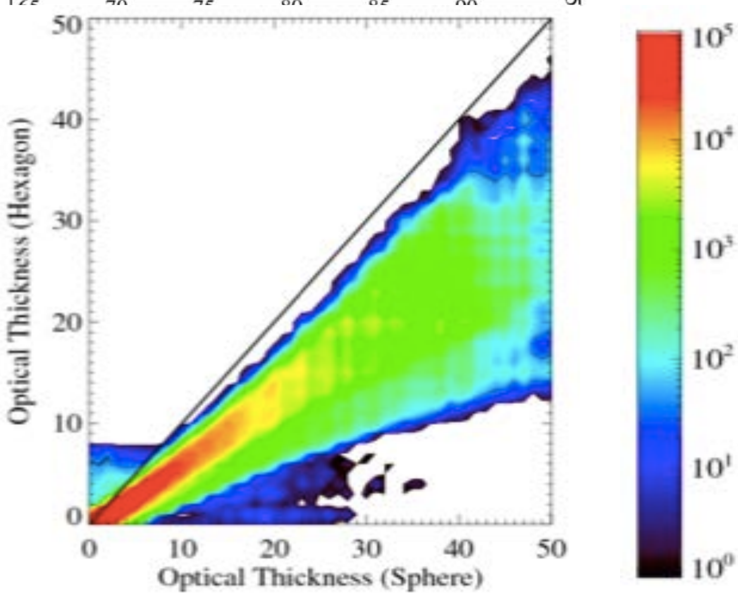

Ice Spheres

Simulated polarized reflectivity vs POLDER observations

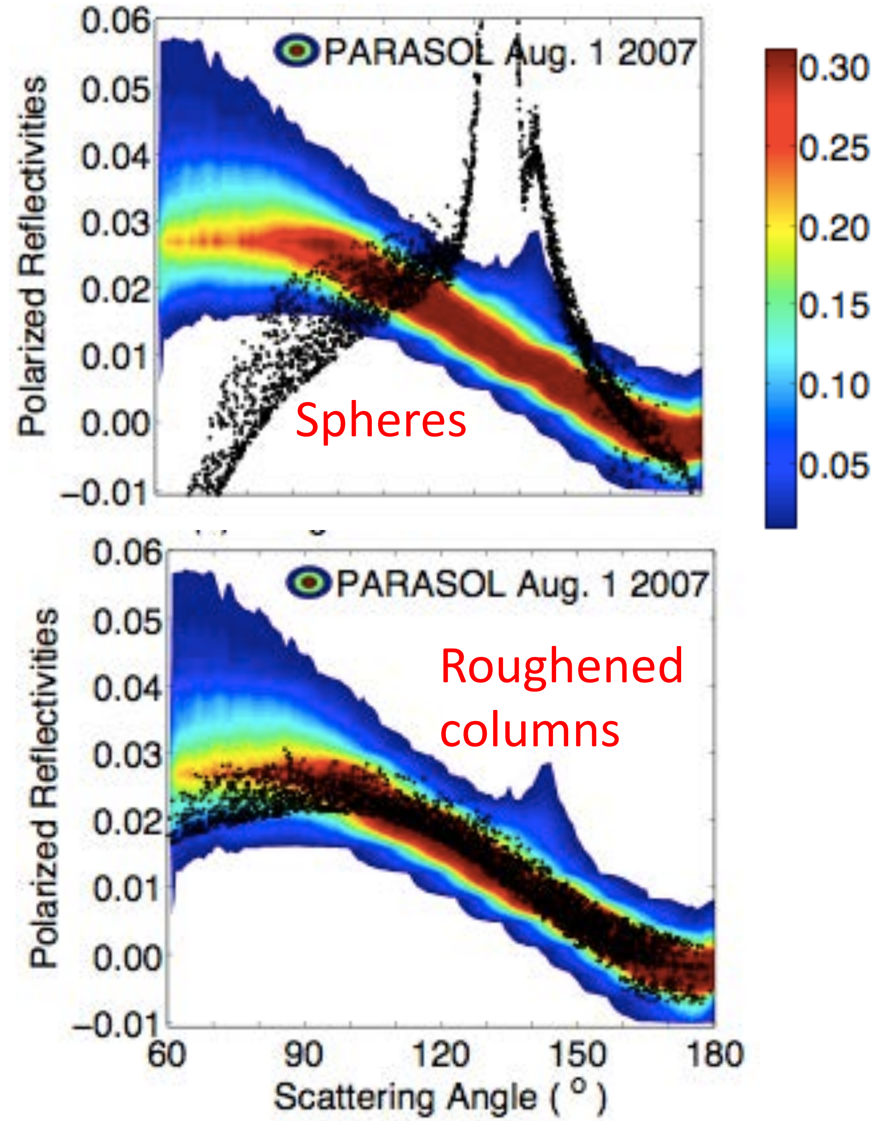

Technical readiness

Modeling capabilities for computing the optical properties of nonspherical ice crystals

Finite-difference Time Domain (FDTD) Method
(Yee 1966; Taflove and Hagness 2000; Yang and Liou, 1996; …)

Second order central difference scheme applied to the time-dependent Maxwell curl equations:

$$\nabla \times \mathbf{H}(\mathbf{r},t) = \frac{\varepsilon}{c}\frac{\partial \mathbf{E}(\mathbf{r},t)}{\partial t} + \frac{4\pi}{c}\sigma \mathbf{E}(\mathbf{r},t),$$

$$\nabla \times \mathbf{E}(\mathbf{r},t) = -\frac{1}{c}\frac{\partial \mathbf{H}(\mathbf{r},t)}{\partial t},$$

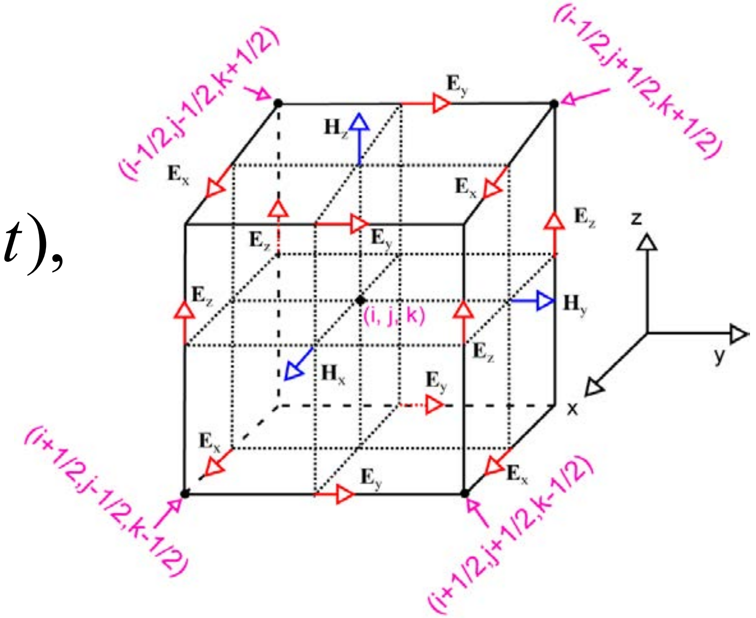

Staggered locations of the E & H field components on a cubic cell (Yee, 1966).

For example, the finite-difference analog of Maxwell's curl equation for the magnetic field:

$$\mathbf{H}^{n+1/2}(\mathbf{r}) = \mathbf{H}^{n-1/2}(\mathbf{r}) - c\Delta t \nabla \times \mathbf{E}^{n}(\mathbf{r}).$$

Finite-difference Time Domain (FDTD) Method

Yee, K. S., 1966: Numerical solution of initial boundary value problems involving Maxwell's equations in isotropic media. IEEE Trans. Antennas Progag., AP-14, 302-307.

As of 10/10/2018: 8,131 citations

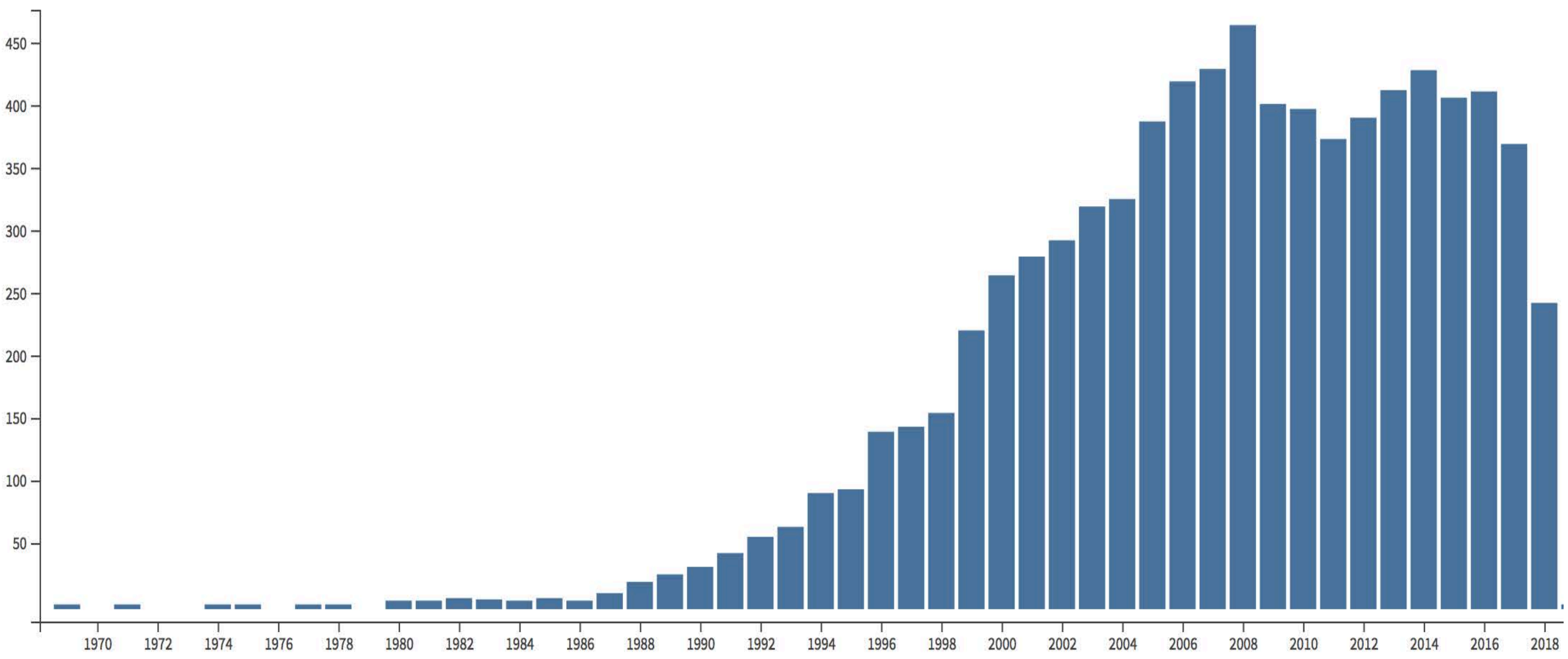

Discrete Dipole Approximation (DDA) Method

(Purcell and Pennypacker 1996; Draine and Flau1994; Yurkin and Hoekstra 2011;…)

Edward Mills Purcell
Nobel Laureate 1952

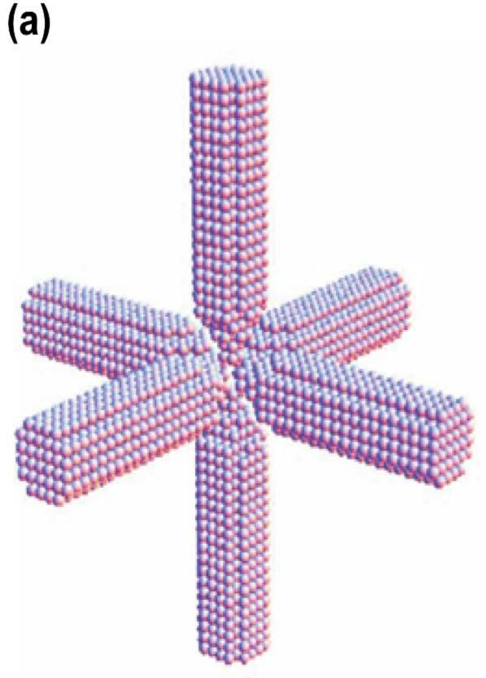

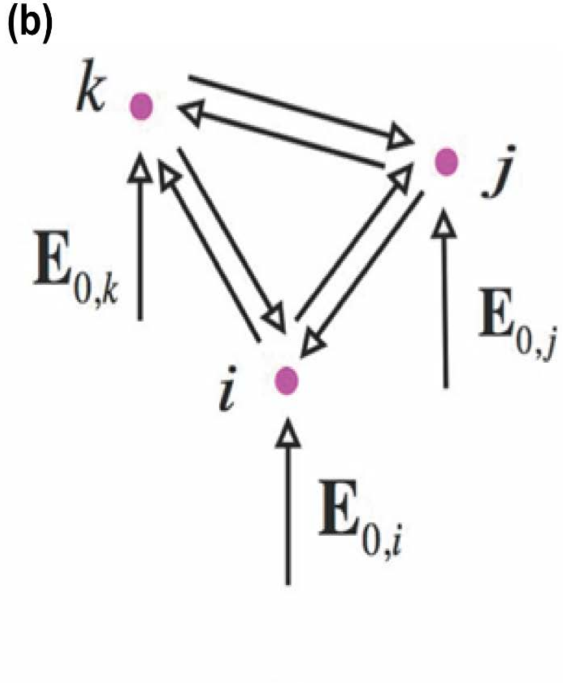

$$\mathbf{P}(\mathbf{r}) == \alpha \mathbf{E}(\mathbf{r})$$

The Clausius-Mossotti (or Lorentz-Lorenz) relation (Lorentz 1880, Lorenz 1880):

$$\alpha = d^3 \frac{3}{4\pi} \frac{m^2-1}{m^2+2}, d = \text{dipole length}$$

$$\mathbf{P}_i = \alpha_i \left(\mathbf{E}_{0,i} + \sum_{i \neq j} \mathbf{A}_{ij} \cdot \mathbf{P}_j \right)$$

$$\sigma_{ext} = \frac{4\pi k}{|E_0|^2} \sum_{j=1}^{N} \mathrm{Im}\left(\mathbf{E}_{0,j}^{*} \cdot \mathbf{P}_j \right)$$

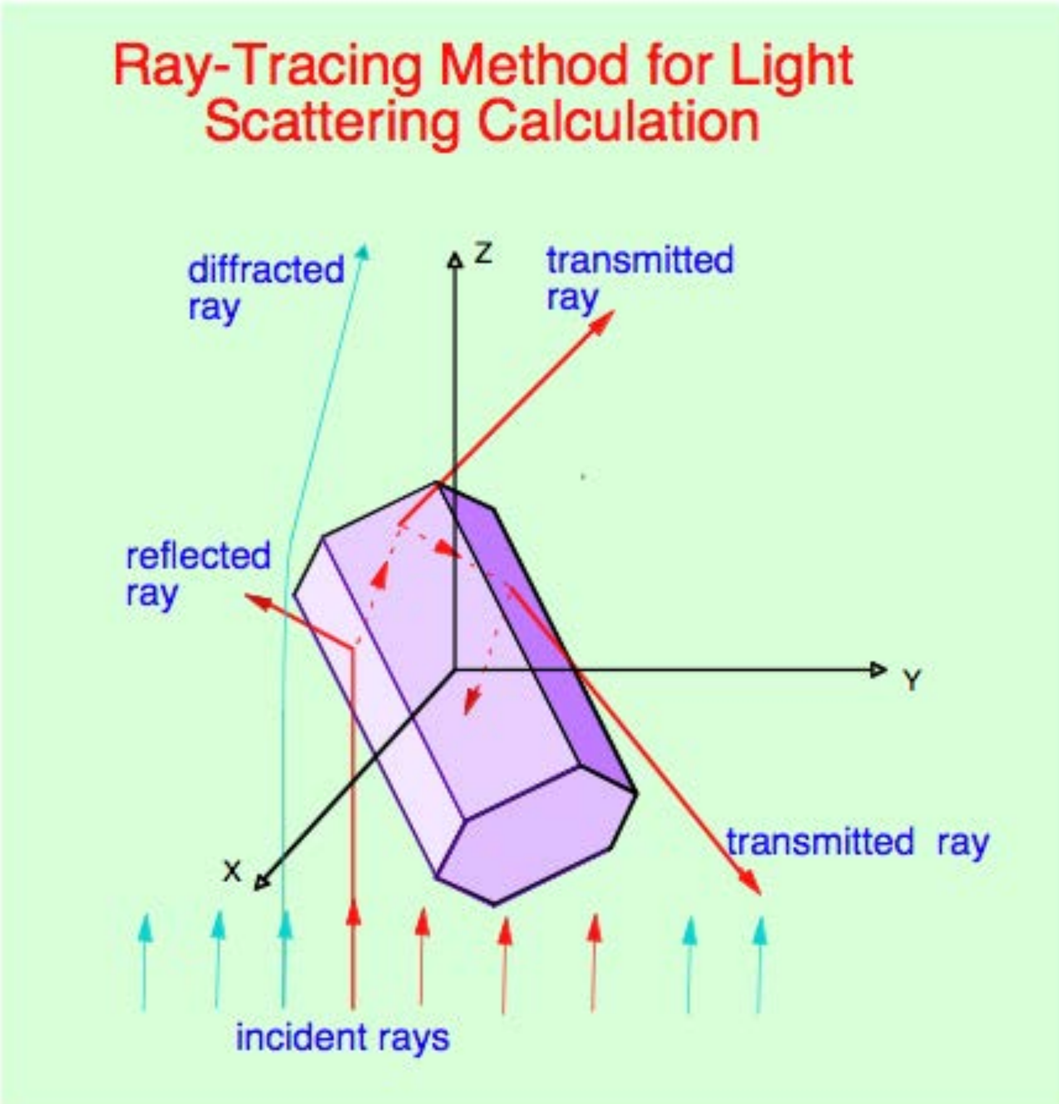

Conventional Geometric Optics Method

Cai, Q., and K. N. Liou, 1982: Polarized light scattering by hexagonal ice crystals: theory. *Appl. Opt.*, 21, 3569–3580.

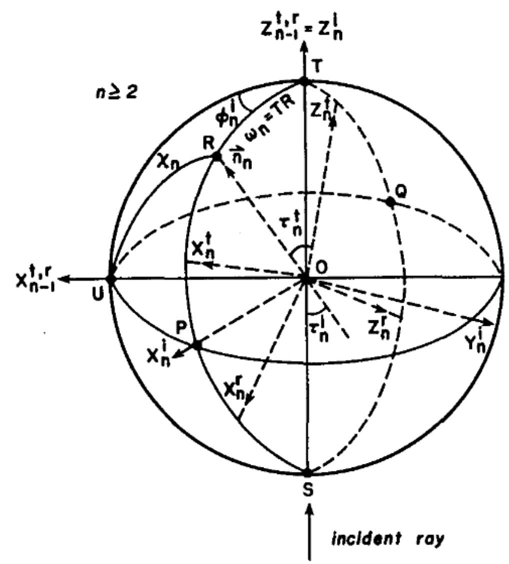

- Constant extinction efficiency, 2
- Singularity
- Artificial separation of contributions by diffraction and geometric rays

Wendling et al. 1979; Cai and Liou, 1982; Takano and Liou, 1989; Mack 1993; Macke et al. 1996; and many others

Applicability of Light-Scattering Computational Methods

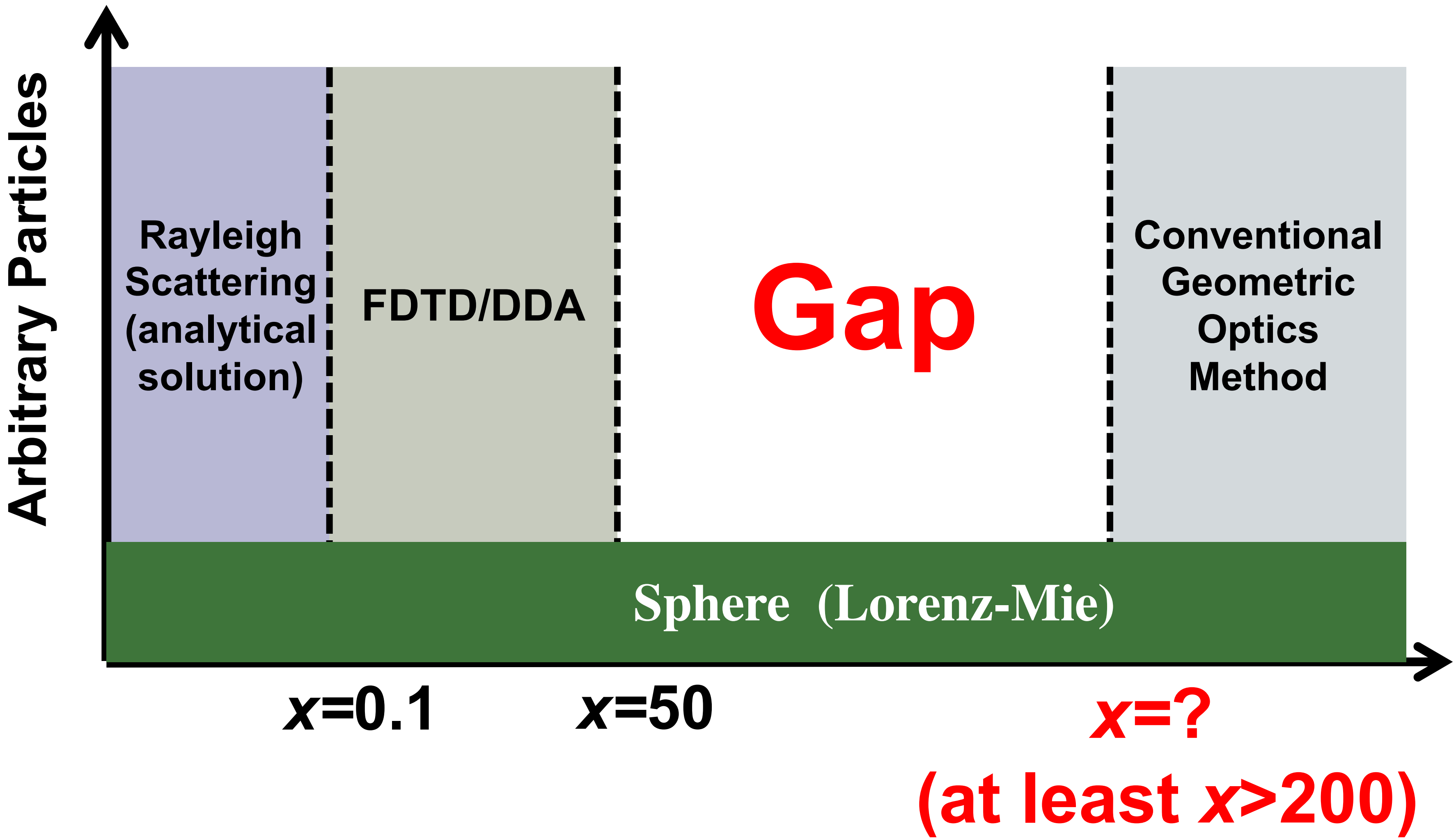

Breakthrough in Light-scattering computation

Invariant Imbedding T-matrix Method (II-TM)

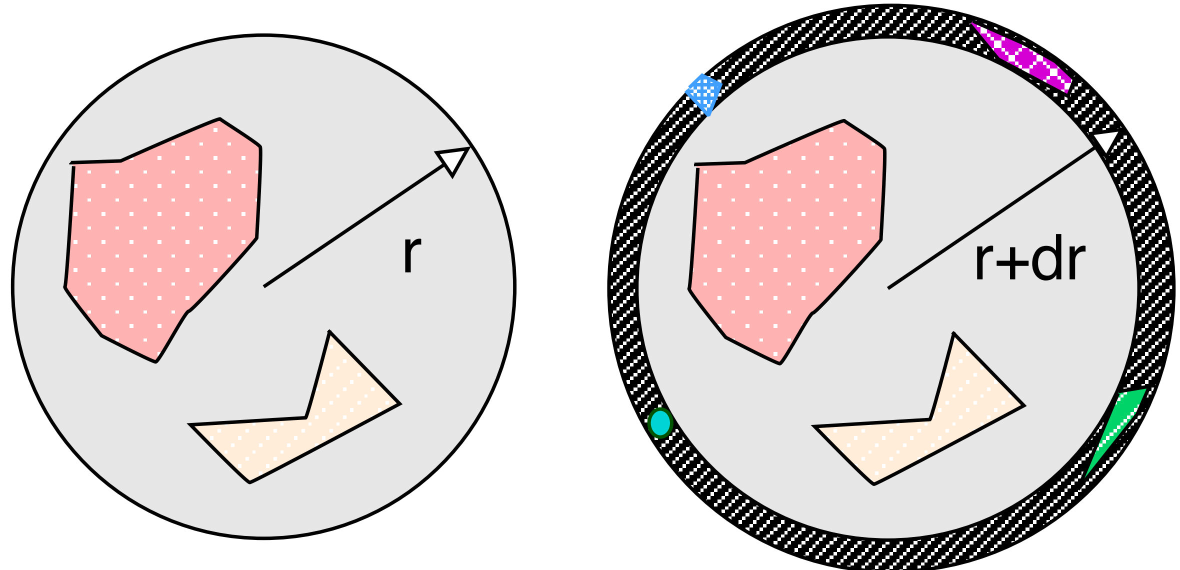

(a) (b)

Maxwell's equations

↓

$$\vec{E}(\vec{r}) = \vec{E}_{inc}(\vec{r}) + k^2 \int (m^2 - 1) \vec{\vec{G}}(\vec{r} - \vec{r}\,') \cdot \vec{E}(\vec{r}\,') d^3\vec{r}\,'$$

Volume Integral Equation

↓

$$T_{mnmn'}(r+dr) = Q_{11}^m(r+dr) + \left[\mathbf{I} + Q_{12}^m(r+dr)\right]\left[\mathbf{I} - T_{mnmn'}(r) Q_{22}^m(r+dr)\right]^{-1} T_{mnmn'}(r)\left[\mathbf{I} + \tilde{Q}_{12}^m(r+dr)\right]$$

Johnson (1988); Bi and Yang (2014)

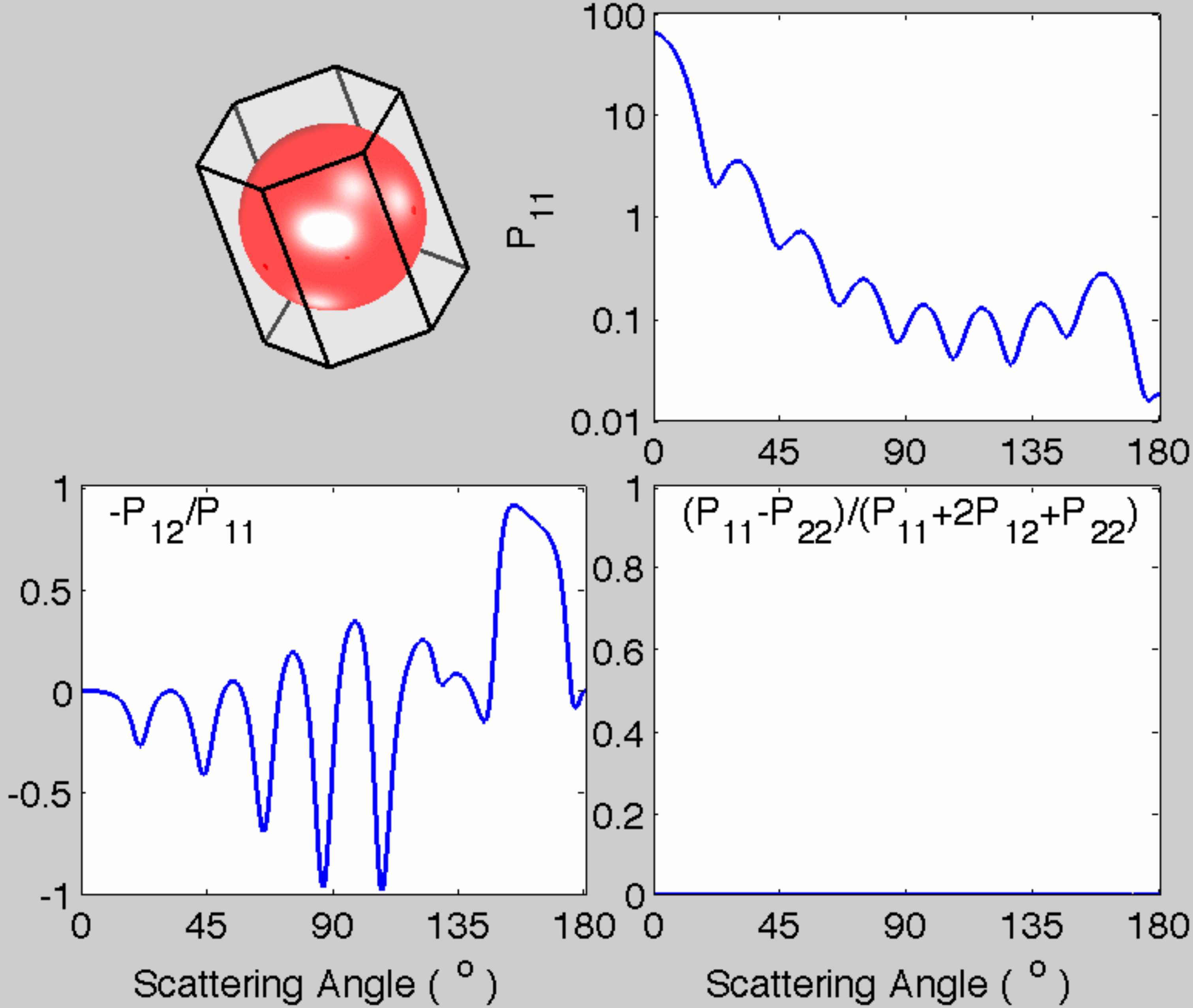

100
10
1
0.1
0.01
P_{11}
0
45
90
135
180
$-P_{12}/P_{11}$
1
0.5
0
-0.5
-1
$(P_{11}-P_{22})/(P_{11}+2P_{12}+P_{22})$
0.8
0.6
0.4
0.2
Scattering Angle (o)
Scattering Angle (o)

Validation

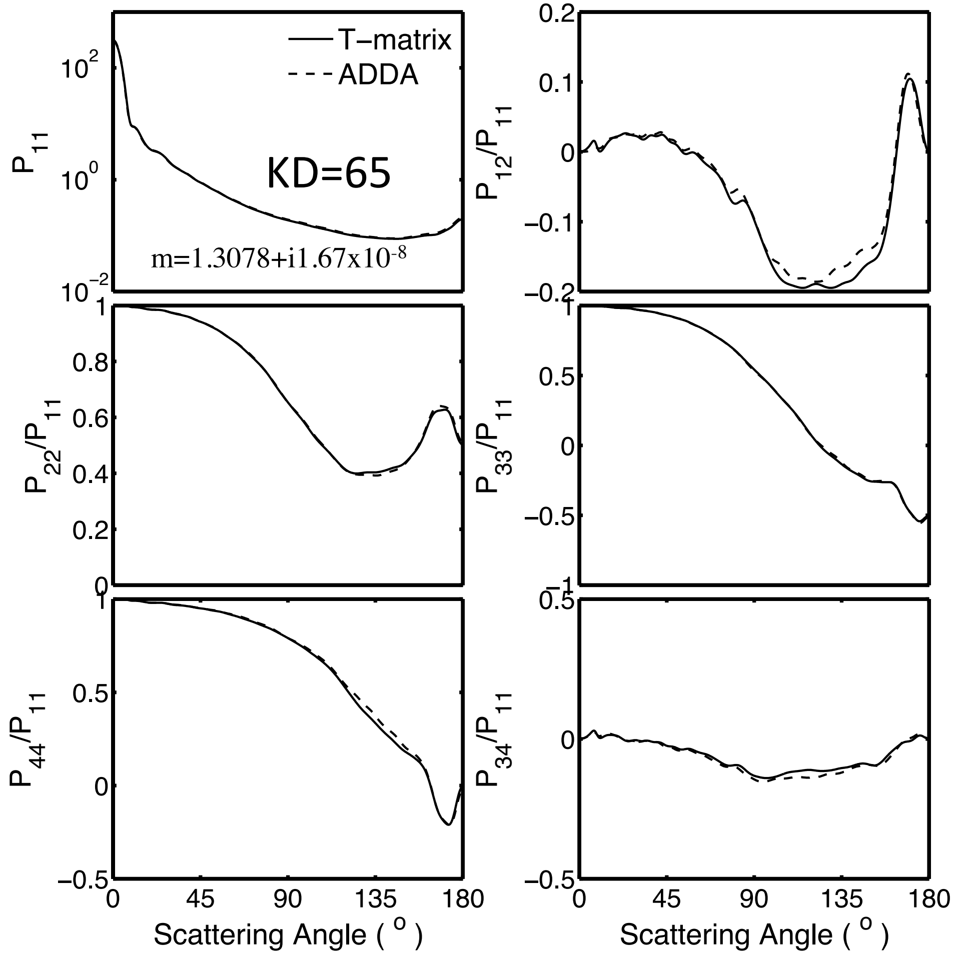

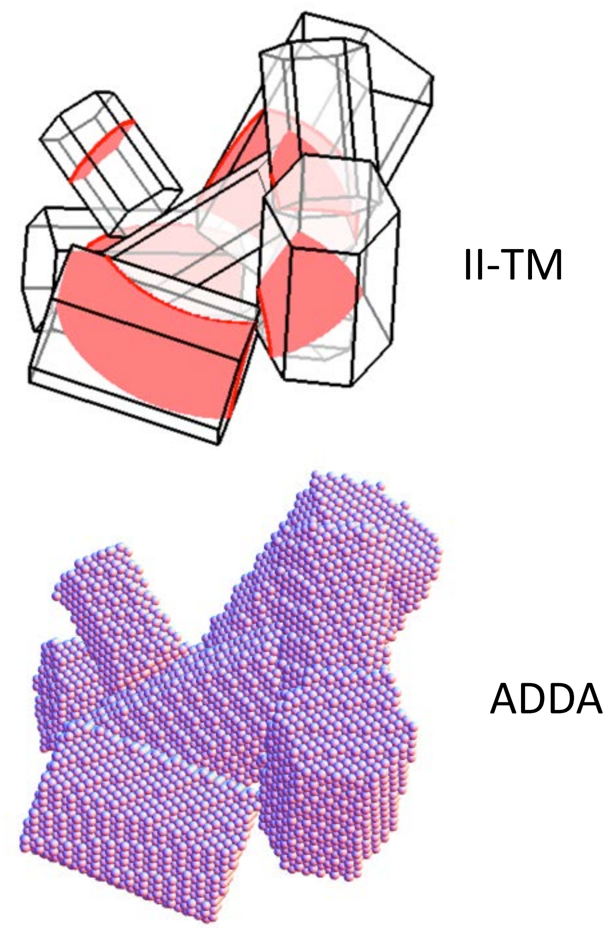

In the ADDA simulation, 1056 orientations with 128 scattering planes are set to achieve the randomness. Bi and Yang (2014).

II-TM is different from the conventional T-matrix method (Extended Boundary Condition Method, EBCM)

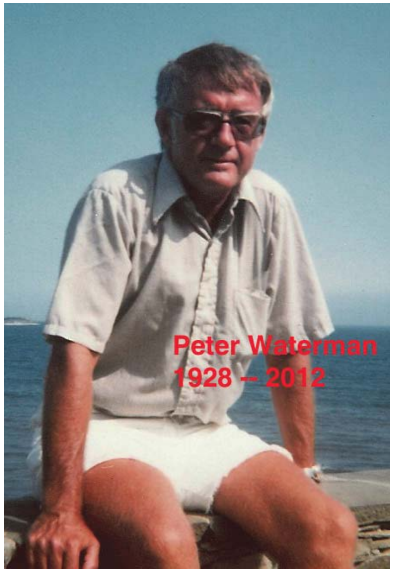

(Mishchenko and Martin, JQSRT, 123:2-7, 2013)

EBCM:

Waterman PC, 1965: Matrix formulation of electromagnetic scattering. Proc. IEEE 53, 805-12

Waterman PC, 1971: Symmetry, unitary, and geometry in electromagnetic scattering. Phys Rev D 3, 825-39

Inscribed sphere

Circumscribing sphere

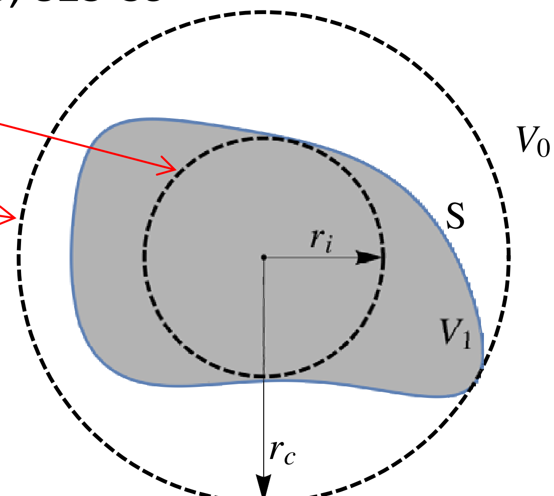

$$\vec{E}^{inc}(\vec{r}') = -\int_s ds\{i\omega\mu_0[\hat{n}\times\vec{H}(\vec{r})]\bullet\overleftrightarrow{G}(\vec{r},\vec{r}') + [\hat{n}\times\vec{E}(\vec{r})]\bullet[\nabla\times\overleftrightarrow{G}(\vec{r},\vec{r}')]\}, \quad \vec{r}'\in V_1$$

$$\vec{E}^{sca}(\vec{r}') = \int_s ds\{i\omega\mu_0[\hat{n}\times\vec{H}(\vec{r})]\bullet\overleftrightarrow{G}(\vec{r},\vec{r}') + [\hat{n}\times\vec{E}(\vec{r})]\bullet[\nabla\times\overleftrightarrow{G}(\vec{r},\vec{r}')]\}, \qquad \vec{r}'\in V_0$$

$$T = -RgQ[Q]^{-1}$$

Surface Integral Equations

For technical details, please see Mishchenko MI, Travis LD and Lacis AA, *Scattering, Absorption, and Emission of Light by Small Particles*. Cambridge: Cambridge University Press; 2002.

Physical-Geometric Optics Method (PGOM)

Yang and Liou (1996)
PGOMS – Surface-integral equation based

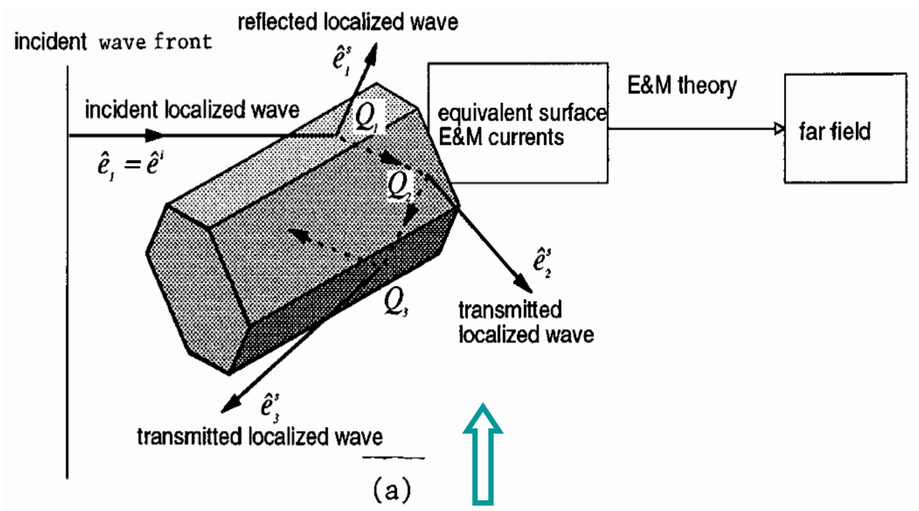

$$\mathbf{E}_s(\mathbf{r})|_{kr\to\infty} = \frac{\exp(ikr)}{-ikr}\frac{k^2}{4\pi}\mathbf{n}\times\iint_S\{\mathbf{n}_S\times\mathbf{E}(\mathbf{r}') - \mathbf{n}\times[\mathbf{n}_S\times\mathbf{H}(\mathbf{r}')]\}\times\exp(-ik\mathbf{n}\cdot\mathbf{r}')\,d^2\mathbf{r}',$$

Yang and Liou (1997)
PGOMV – Volume-integral equation based

$$\mathbf{E}_s(\mathbf{r}) = \frac{k^2\exp(ikr)}{4\pi r}\iiint_V[\varepsilon(\mathbf{r}')-1]\{\mathbf{E}(\mathbf{r}')-\mathbf{n}[\mathbf{n}\cdot\mathbf{E}(\mathbf{r}')]\}\exp(-ik\mathbf{n}\cdot\mathbf{r}')\,d^3\mathbf{r}'.$$

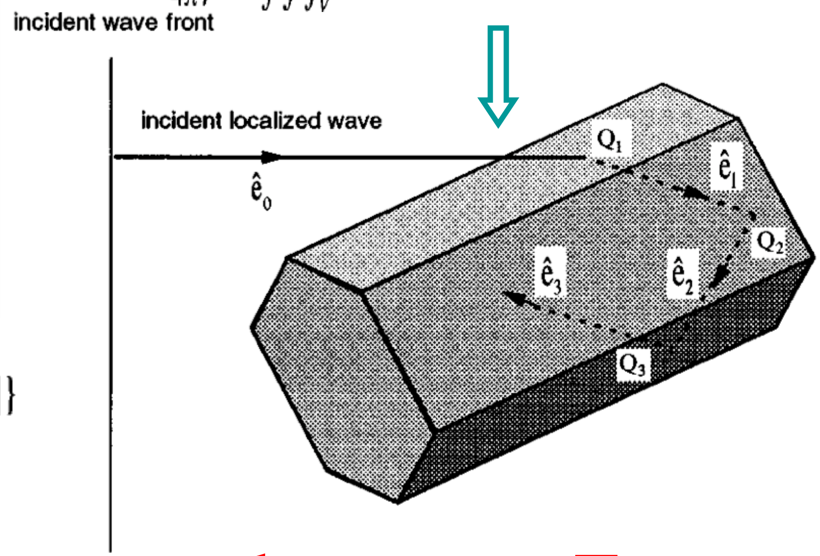

New improvements by our research group at Texas A&M University using computer graphics techniques

PGOMS vs II-TM

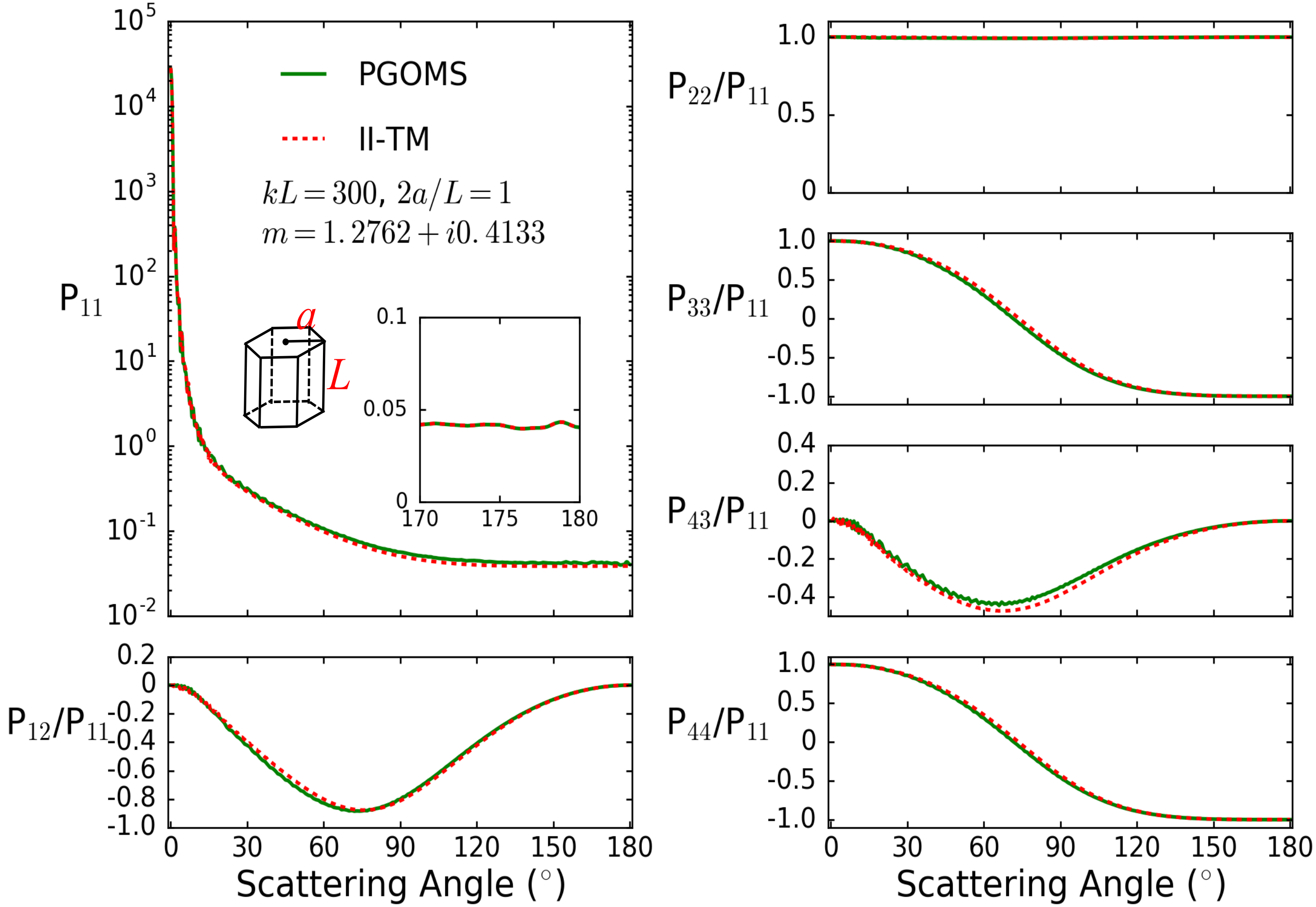

Comparison of the phase matrix elements computed by PGOMS and IITM. The particle is a hexagonal column with aspect ratio 1. The refractive index is 1.2762+*i*0.4133, the ice refractive index at 12μm wavelength. The inset plots show the P_{11} element for 170° -180° scattering angles. The size parameter is kL=300, or ka=150.

PGOMS vs II-TM

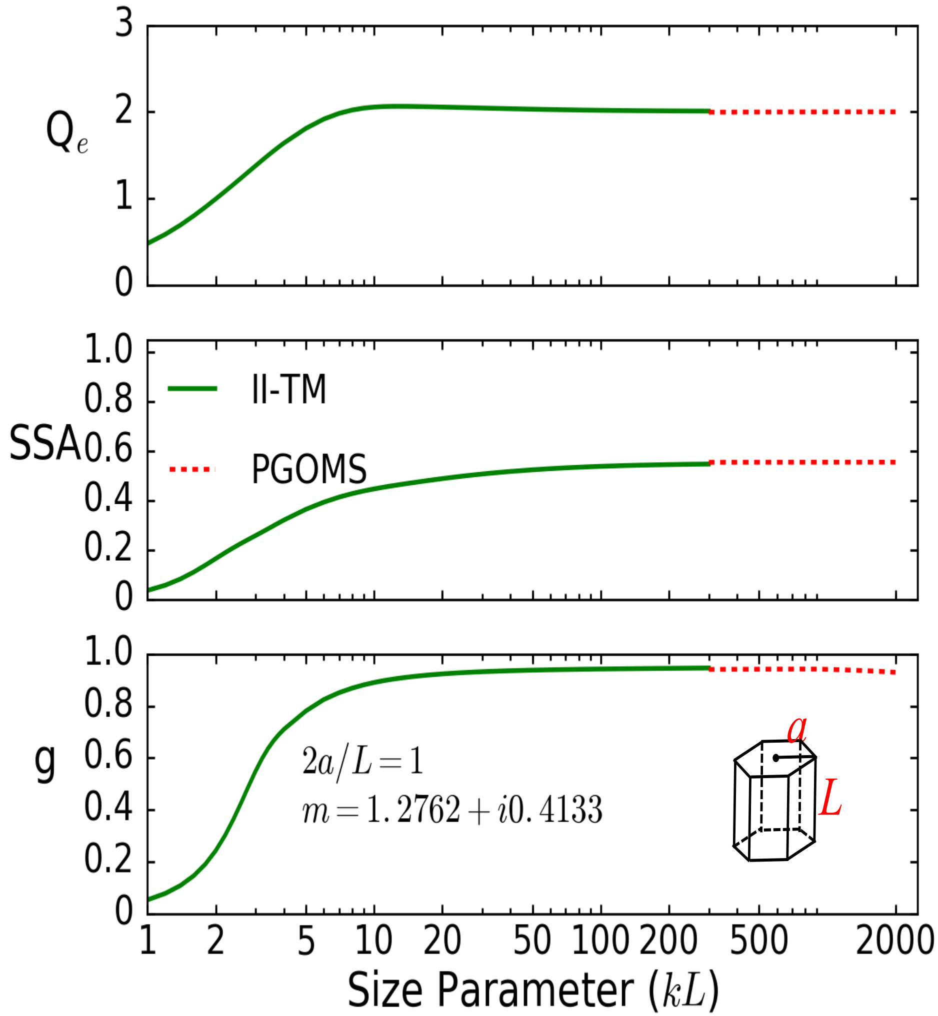

Extinction efficiency (Q_e), single-scattering (SSA), and asymmetry factor (g) computed by II-TM and PGOM. The particle is a hexagonal column with aspect ratio 1. The refractive index is 1.2762+i0.4133 that is the ice refractive index at 12 μm wavelength

Breakthrough: A combination of II-TM and PGOM can accurately cover the entire size parameter region

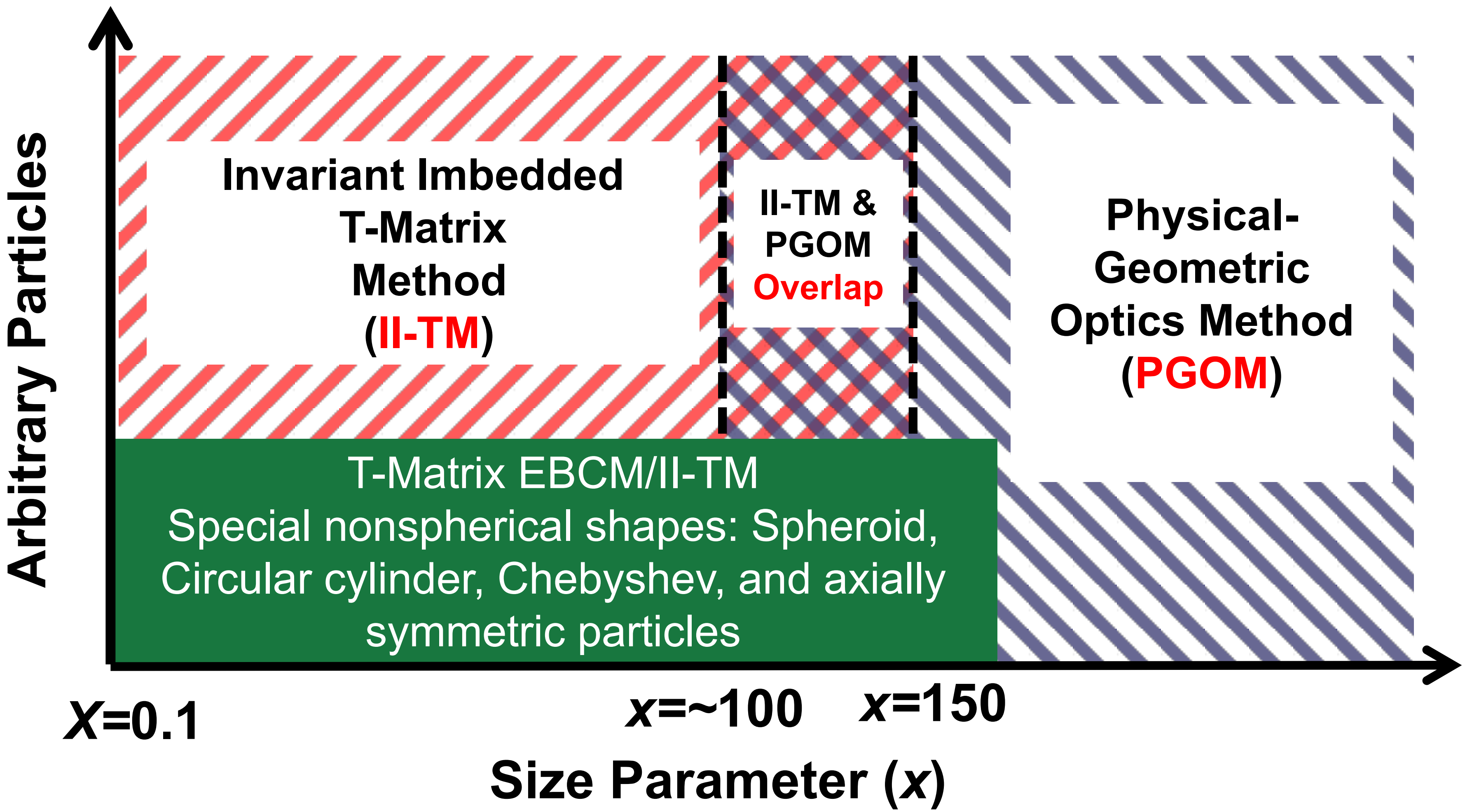

Scattering effect is important in radiative transfer simulation even in the infrared region

The current RRTM-G neglects the scattering effect in LW bands

TOA Upward Flux Biases

TEXAS A&M UNIVERSITY

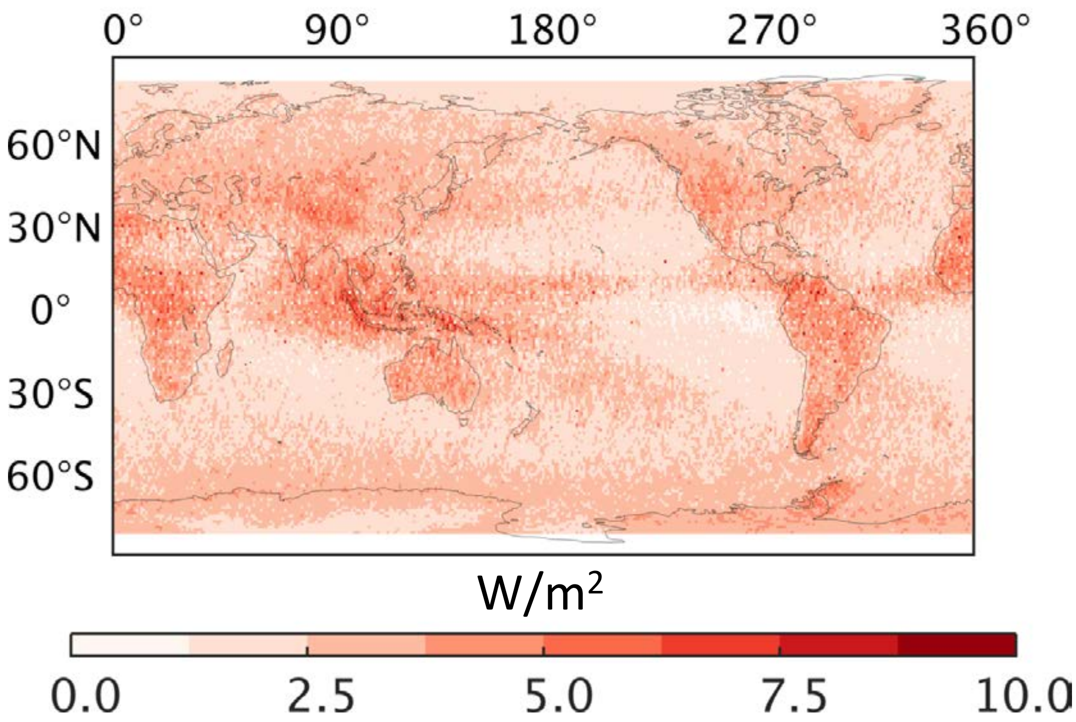

Positive biases mean that the TOA upward fluxes are overestimated when LW scattering is ignored

Areas containing large biases

- **Intertropical Convergence Zone (ITCZ)**
- **Pacific warm pool**
- **Tibetan Plateau**

Large biases (up to 12 W/m^2)

Kuo, C.-P., P. Yang, X. Huang, D. Feldman, M. Flanner, C. Kuo, and E. J. Mlawer, 2017: *Journal of Advances in Modeling Earth Systems*.

Surface Downward Flux Biases

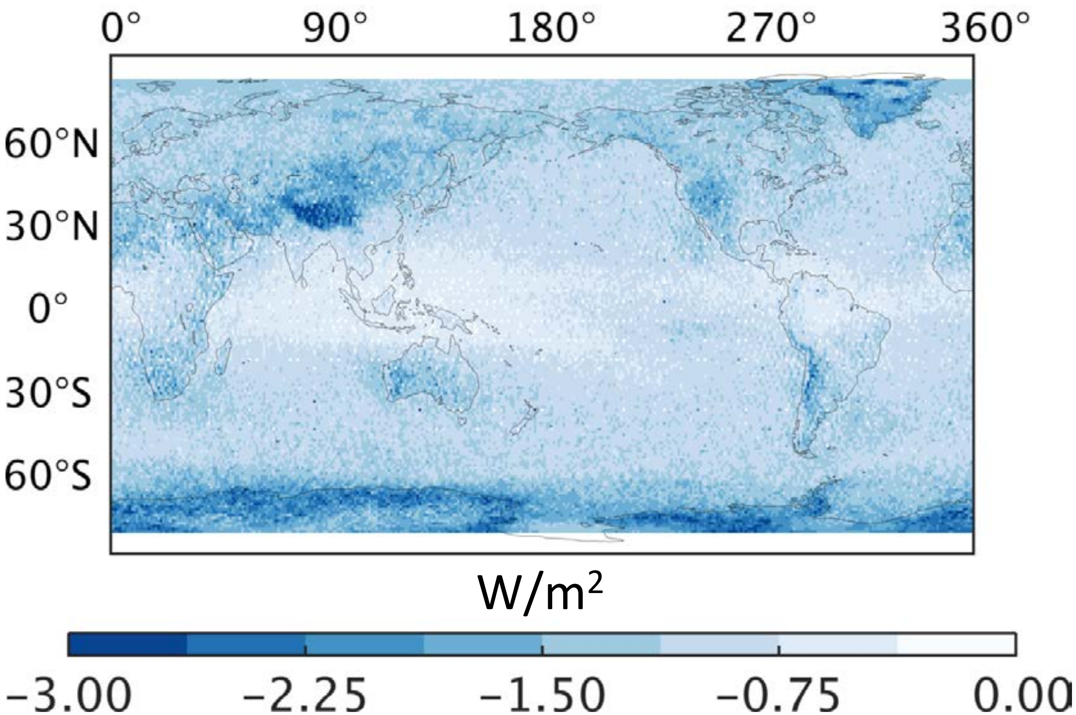

Areas containing large biases

- **Dry and high regions**
- **Tibetan Plateau**
- **Antarctic**
- **Greenland**

Large biases (~-3.6 W/m^2)

Negative biases mean that the surface downward fluxes are underestimated when LW scattering is ignored

Kuo, C.-P., P. Yang, X. Huang, D. Feldman, M. Flanner, C. Kuo, and E. J. Mlawer, 2017: *Journal of Advances in Modeling Earth Systems*.

Flux Biases

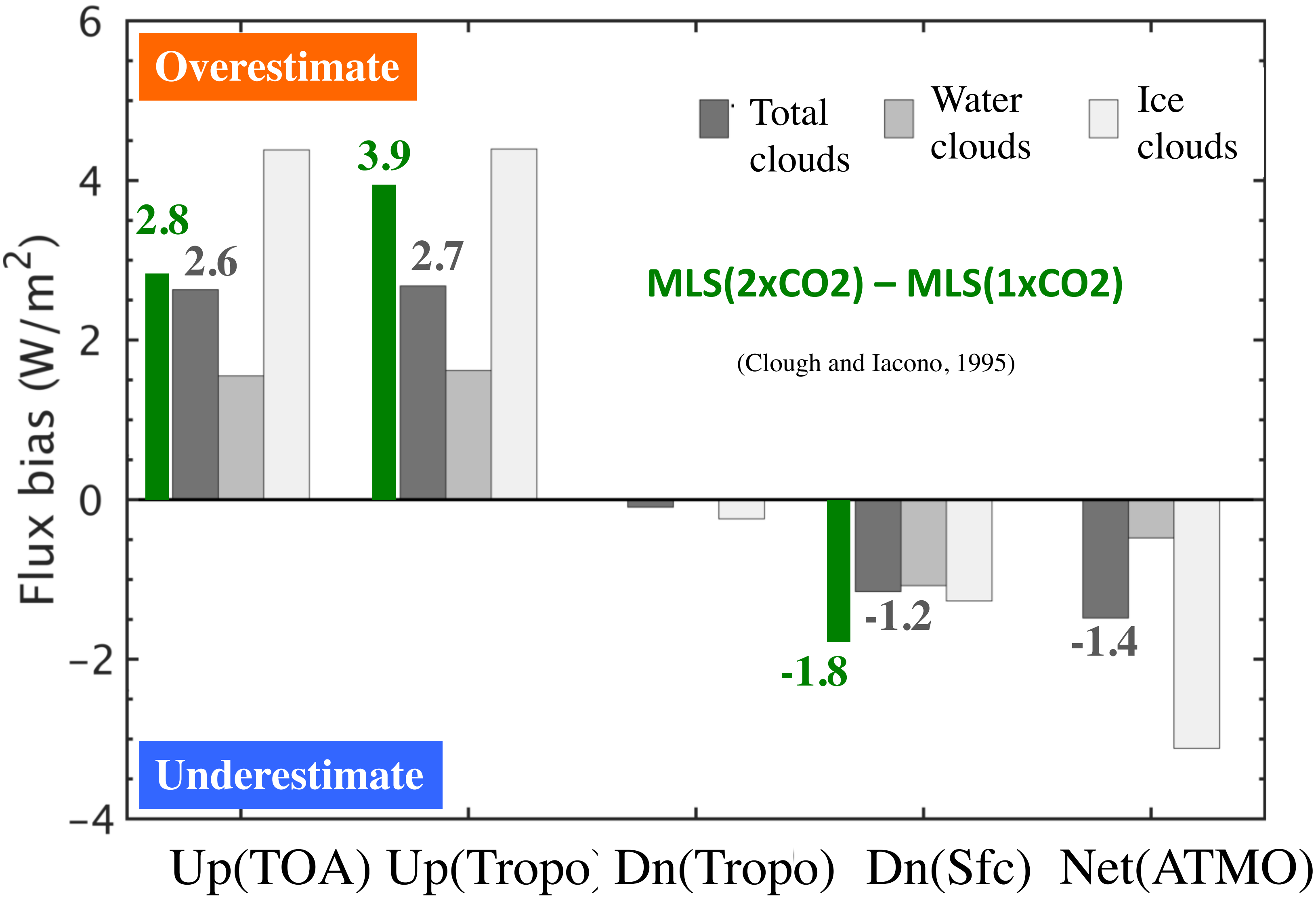

6
4
2
0
−2
−4
Flux bias (W/m^2)
Overestimate
Underestimate
Total clouds
Water clouds
Ice clouds
2.8
2.6
3.9
2.7
-1.8
-1.2
-1.4
MLS(2xCO2) – MLS(1xCO2)
(Clough and Iacono, 1995)
Up(TOA)
Up(Tropo)
Dn(Tropo)
Dn(Sfc)
Net(ATMO)

Spectral Analyses

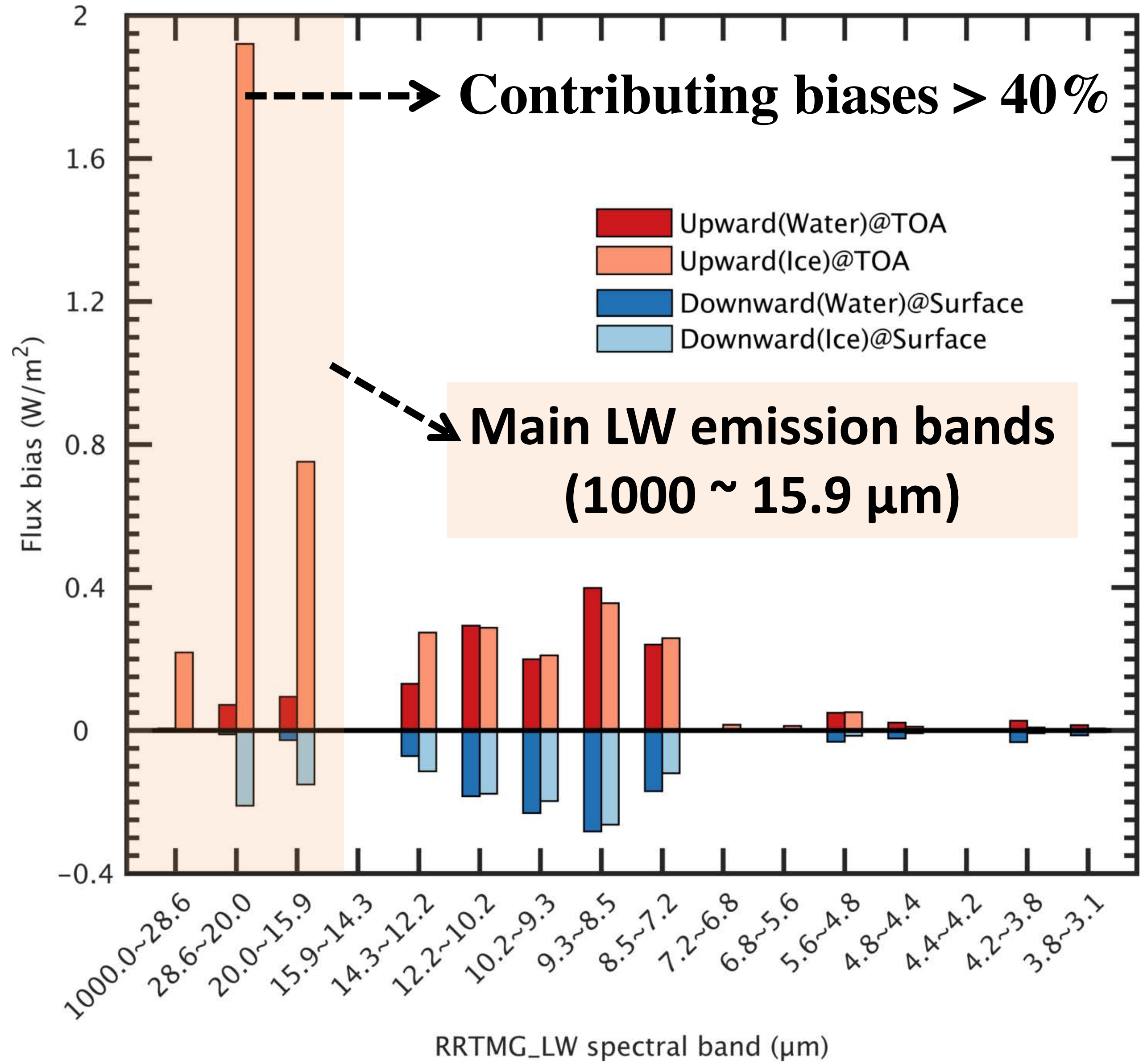

Spectral Analyses

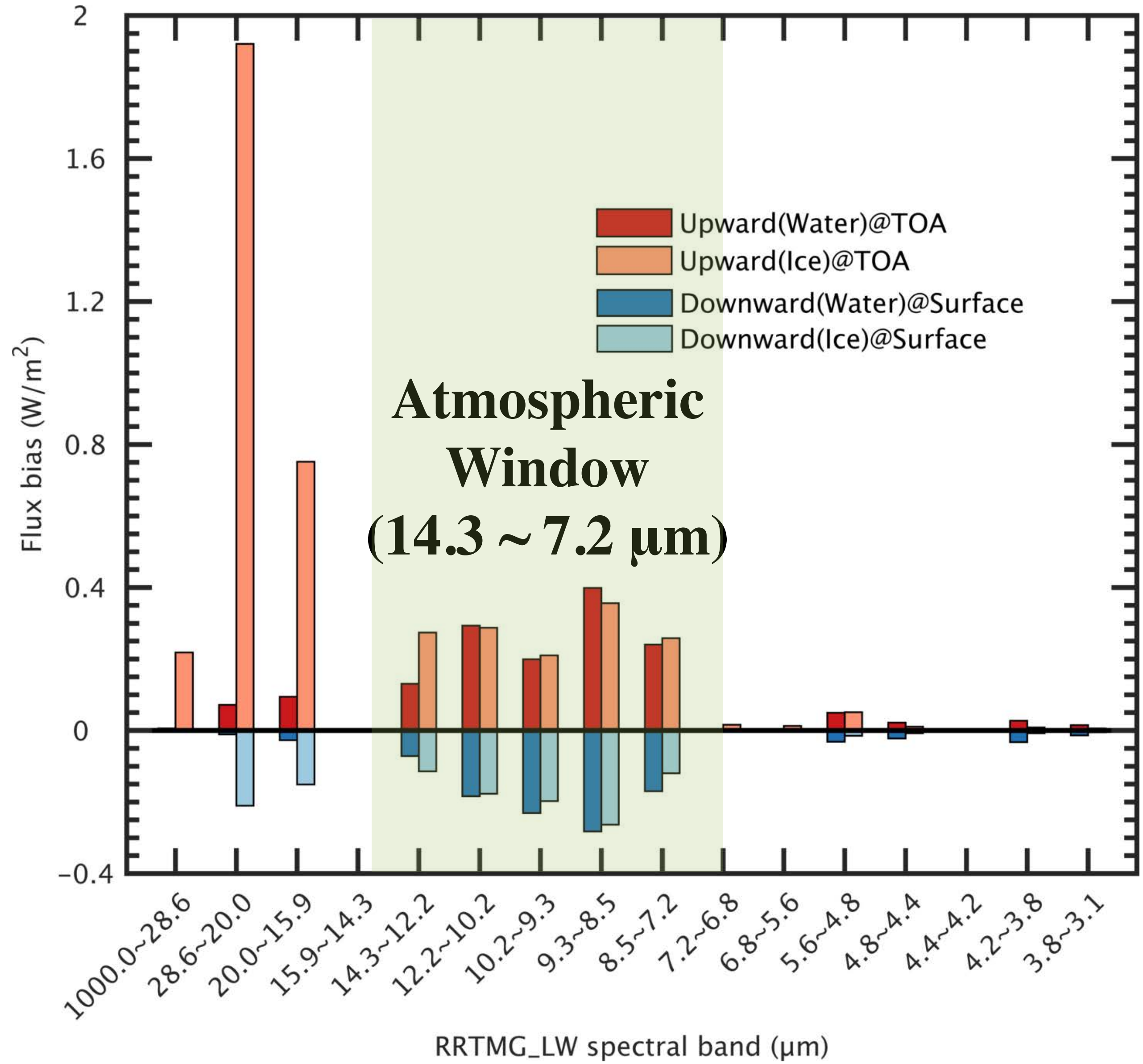

Spectral Analyses

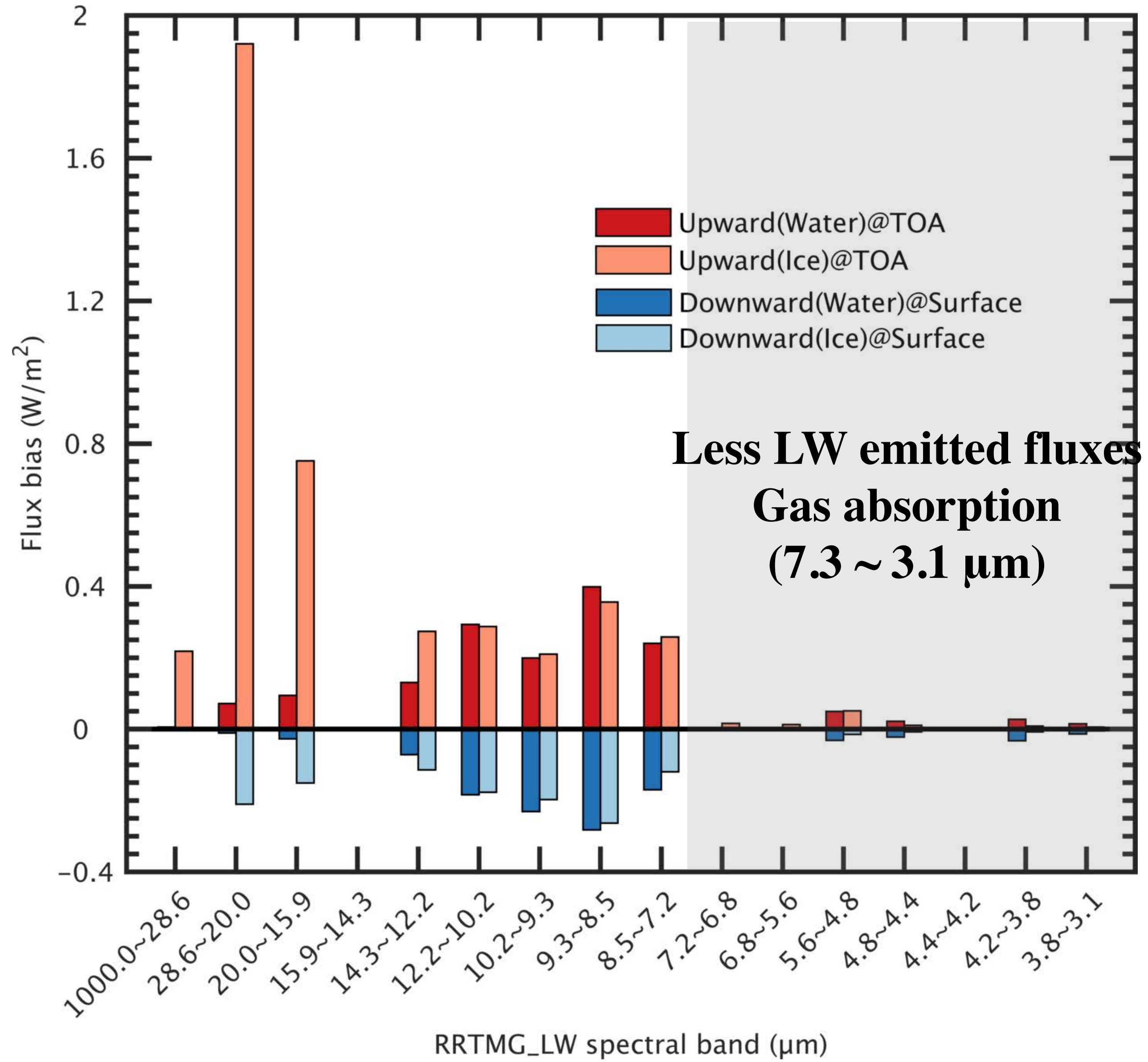

MODIS Ice Particle Models (Collections 4, 5, 6)

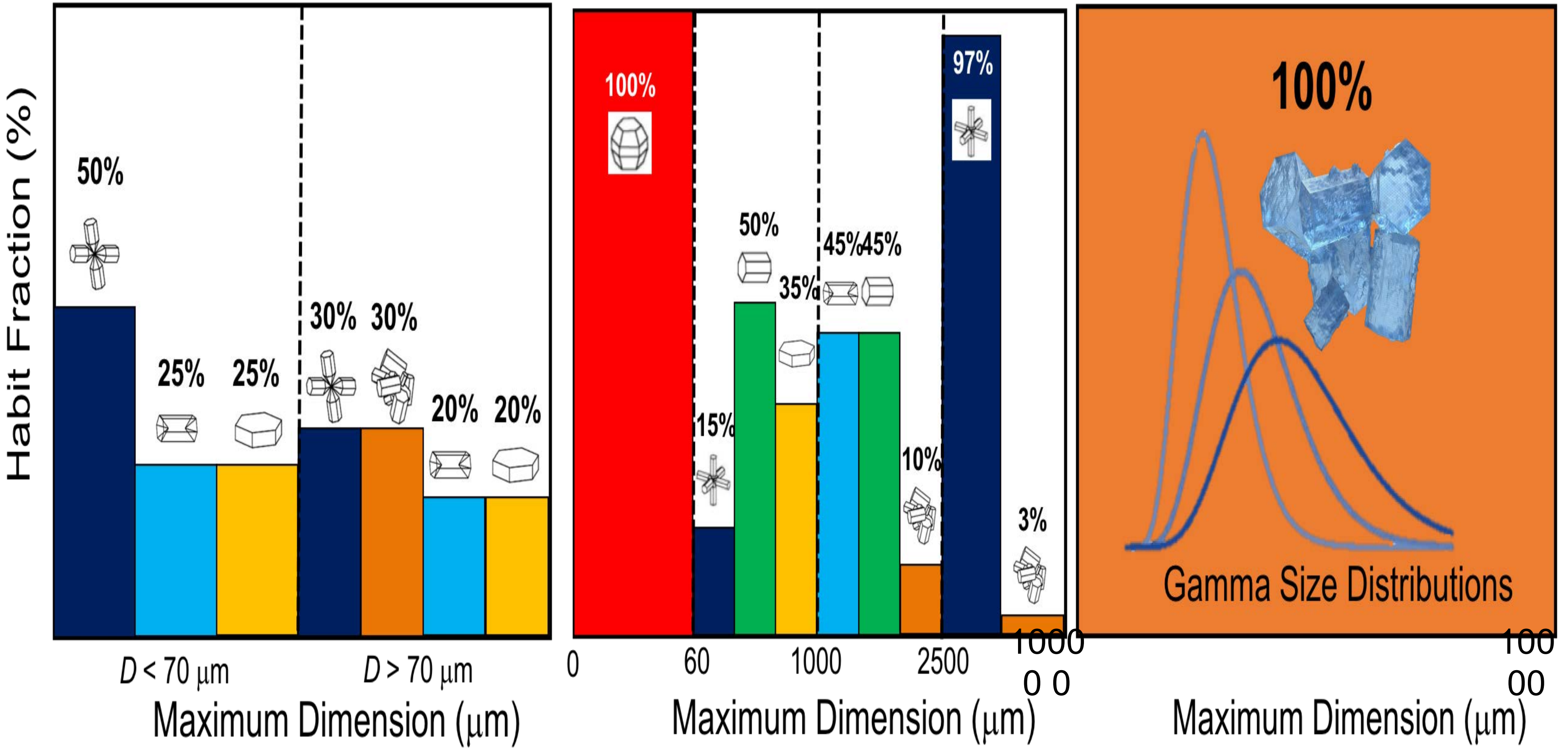

References: King et al. 2004, Baum et al. 2005, Platnick et al. 2017

CERES ice particle models (Editions 2-4, and a two-habit model for future Edition 5)

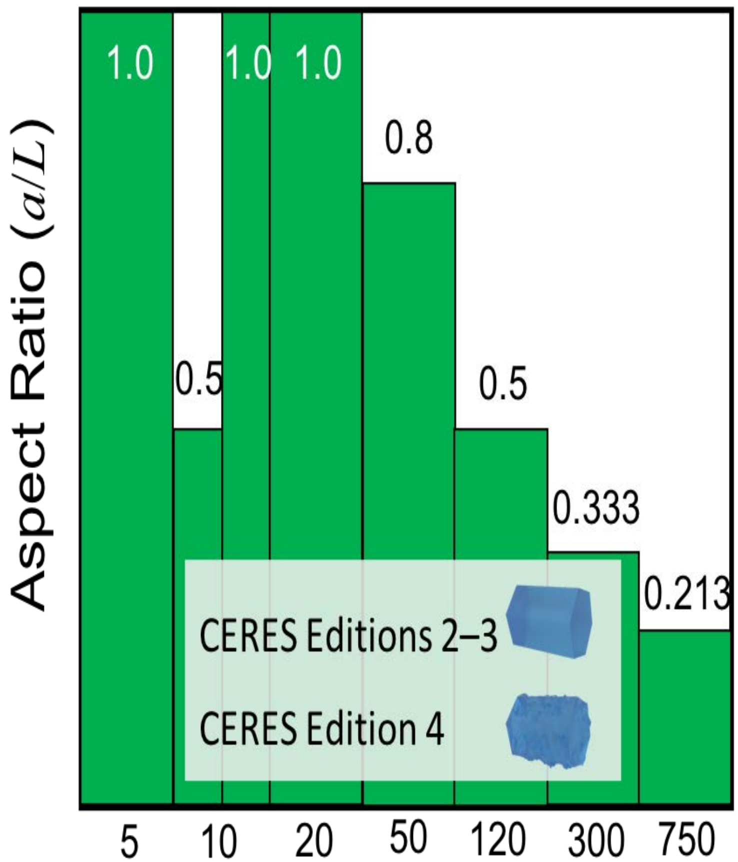

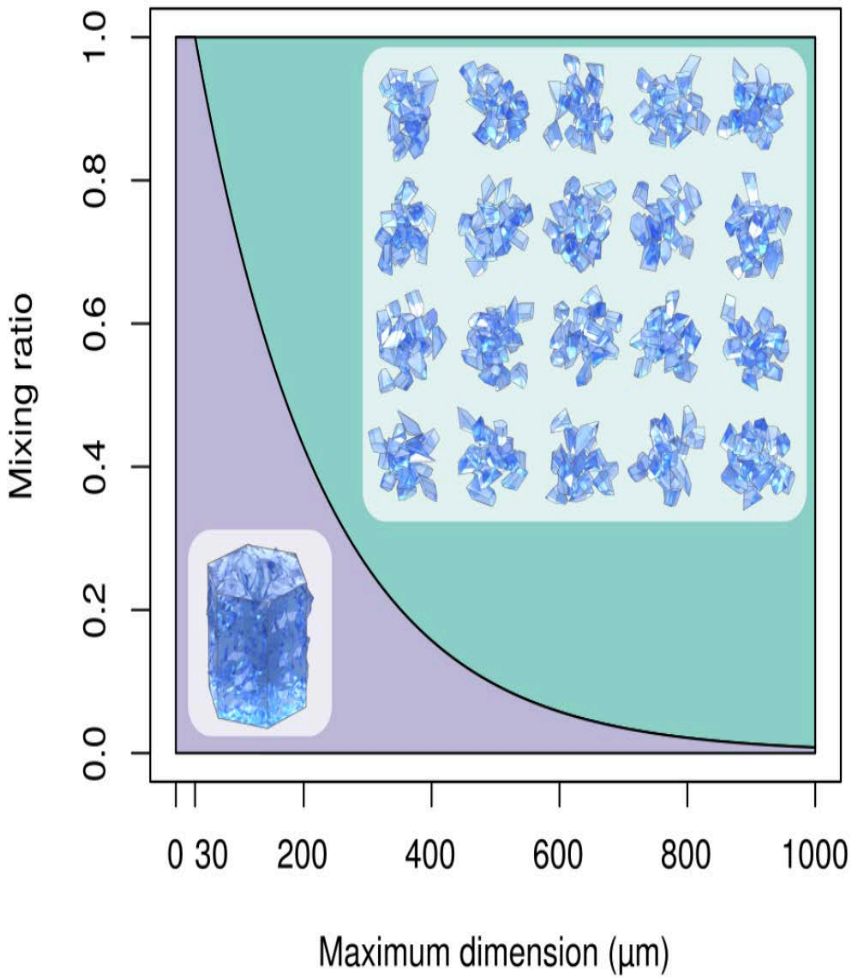

References: Minnis et al. 1993, 2011; Loeb et al. 2017

Phase Function Comparison

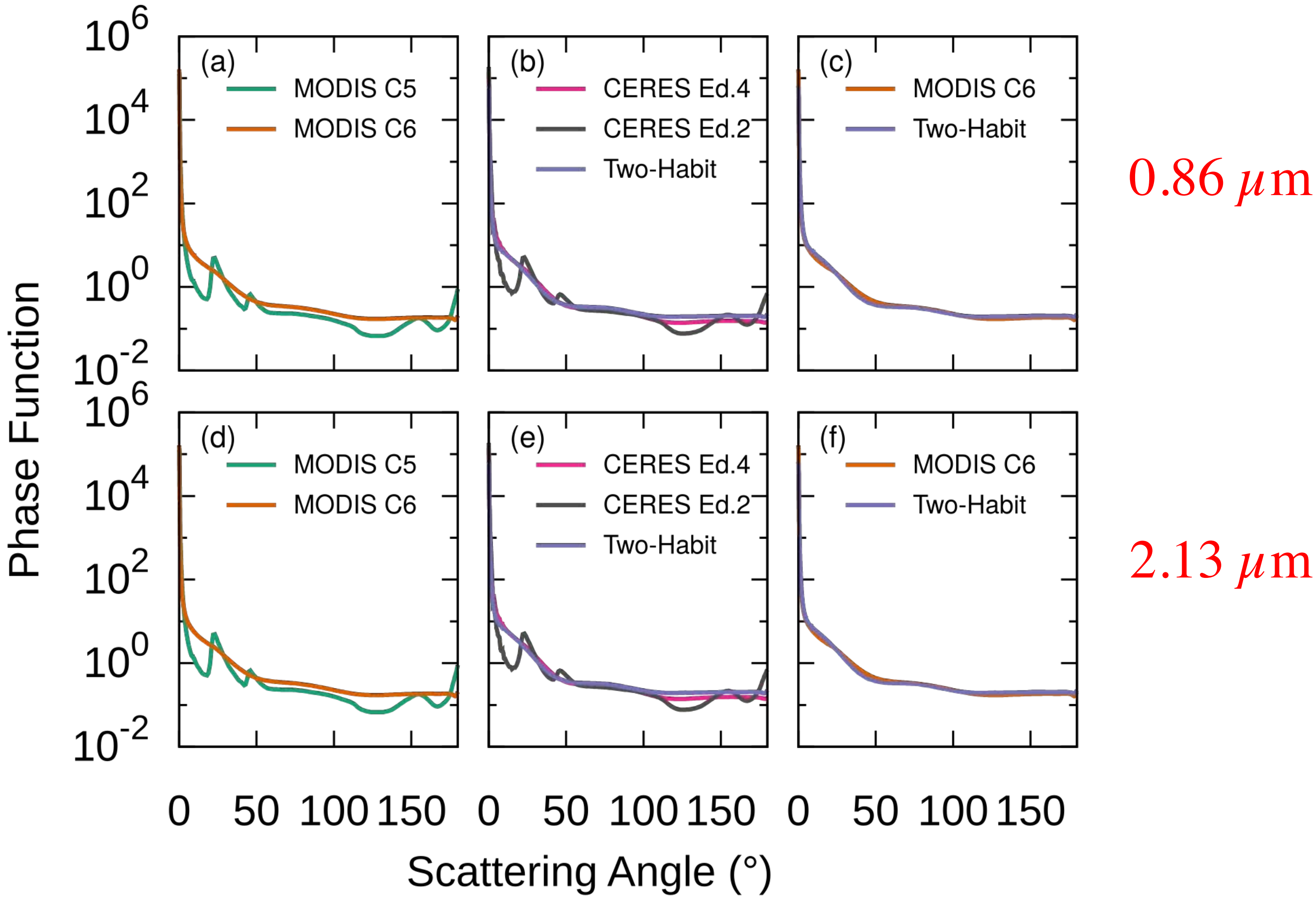

Comparison of the phase functions at wavelength 0.86 µm based on (a) MODIS Collection 4, 5, and 6; (b) CERES Edition 2, 4, and the Two-habit model; and (c) MODIS Collection 6 and the Two-habit model. Diagrams (d), (e), and (f) in bottom rows are counterpart of (a), (b), (c) at wavelength 2.13 µm. Effective radius is fixed at 30 µm.

Asymmetry Factor Comparison

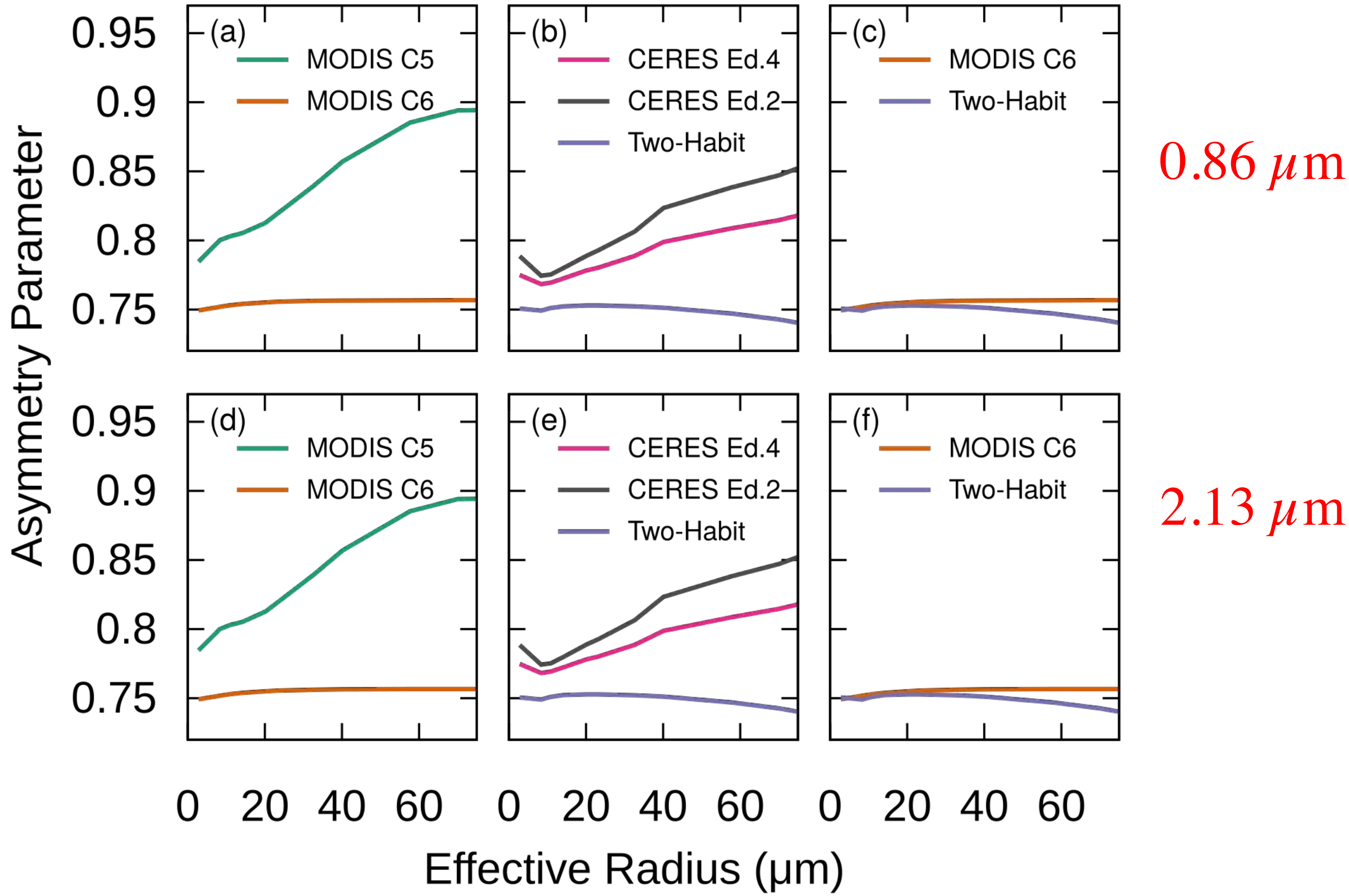

Comparison of the asymmetry parameter at wavelength 0.86 μm based on (a) MODIS Collection 4, 5, and 6; (b) CERES Edition 2, 4, and the Two-habit model; and (c) MODIS Collection 6 and the Two-habit model. Diagrams (d), (e), and (f) in bottom rows are counterpart of (a), (b), (c) at wavelength 2.13 μm. Effective radius is fixed at 30 μm.

The similarity relation at a non-absorptive wavelength (van de Hulst 1971, 1974)

$$(1-g)\,\tau=(1-g')\,\tau'$$

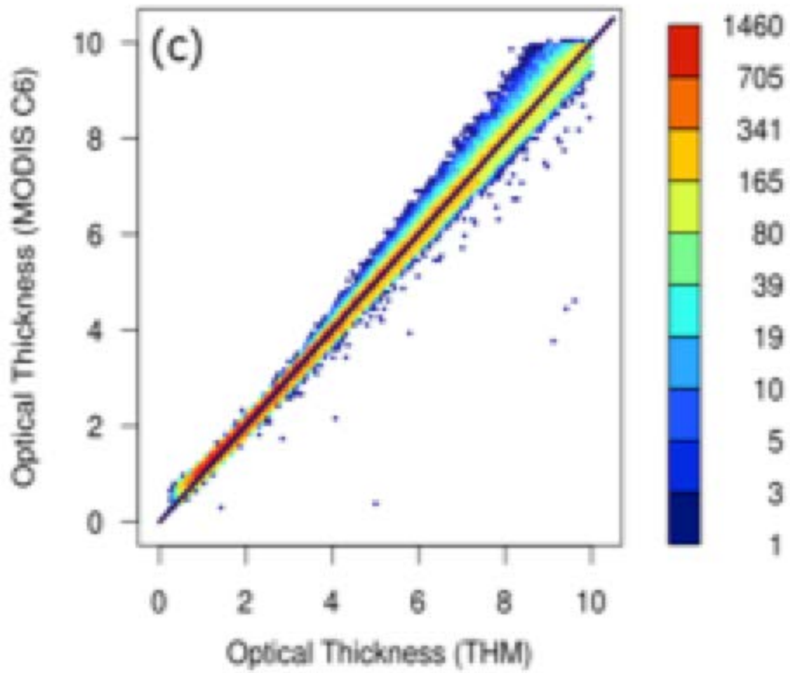

Thus

$g_{C6} \cong g_{THM}$ leads to $\tau_{C6} \cong \tau_{THM}$

$g_{C5} > g_{C6}$ leads to $\tau_{C5} > \tau_{C6}$

Spectral consistency

- *Nakajima-King bispectral method based on two solar bands*
- *Split window technique based on thermal infrared bands*

Retrievals based on the two methods should be consistent!

Consistency Check (VIS-NIR vs IR retrieval techniques)

Sphere

CERES Ed 4

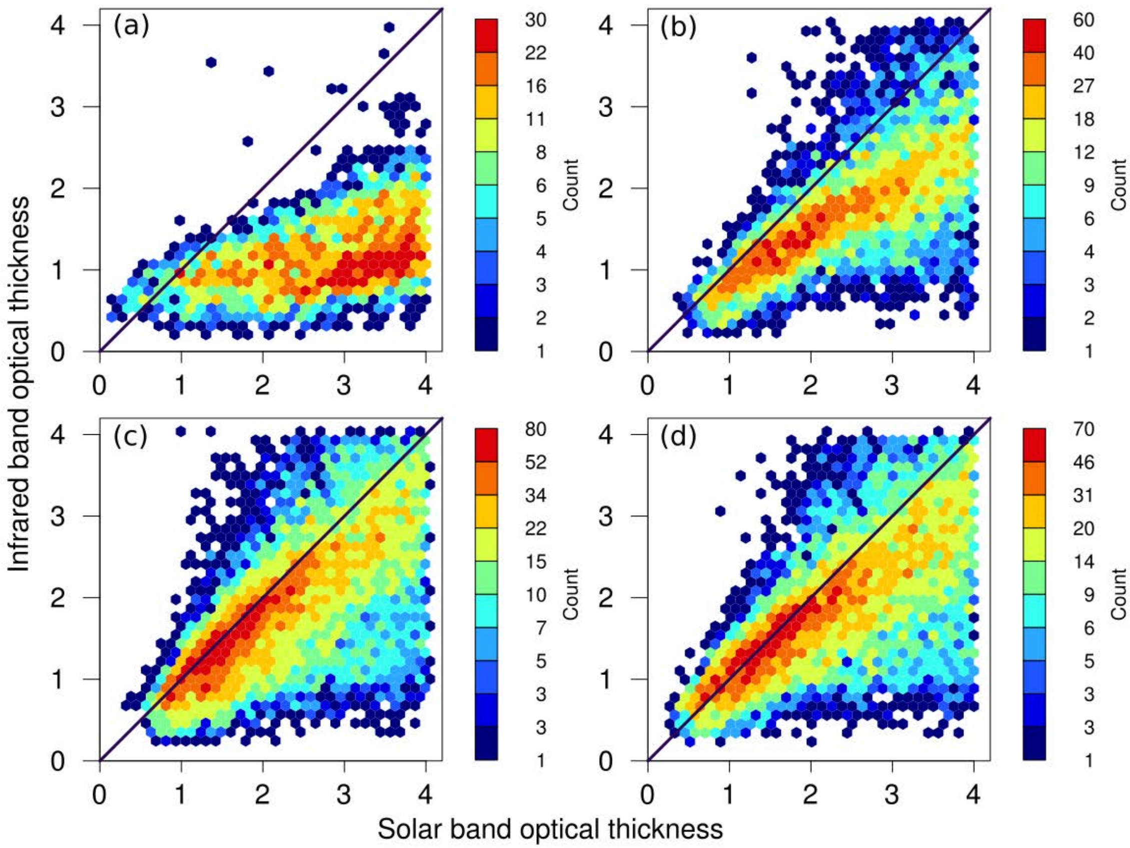

MODIS C6

Two-Habit Model

Comparison of retrieved optical thickness values from a shortwave method (the Nakajima-King bi-spectral method) and a longwave method (the split-window technique). (a) Ice

[Loeb et al.], 2018: Impact of ice microphysics on satellite cloud retrievals and broadband flux radiative transfer model calculations. *J. Climate*, 31, 1851-1864.

Cloud Property Differences at Aqua Overpass Time
(THM minus Smooth)

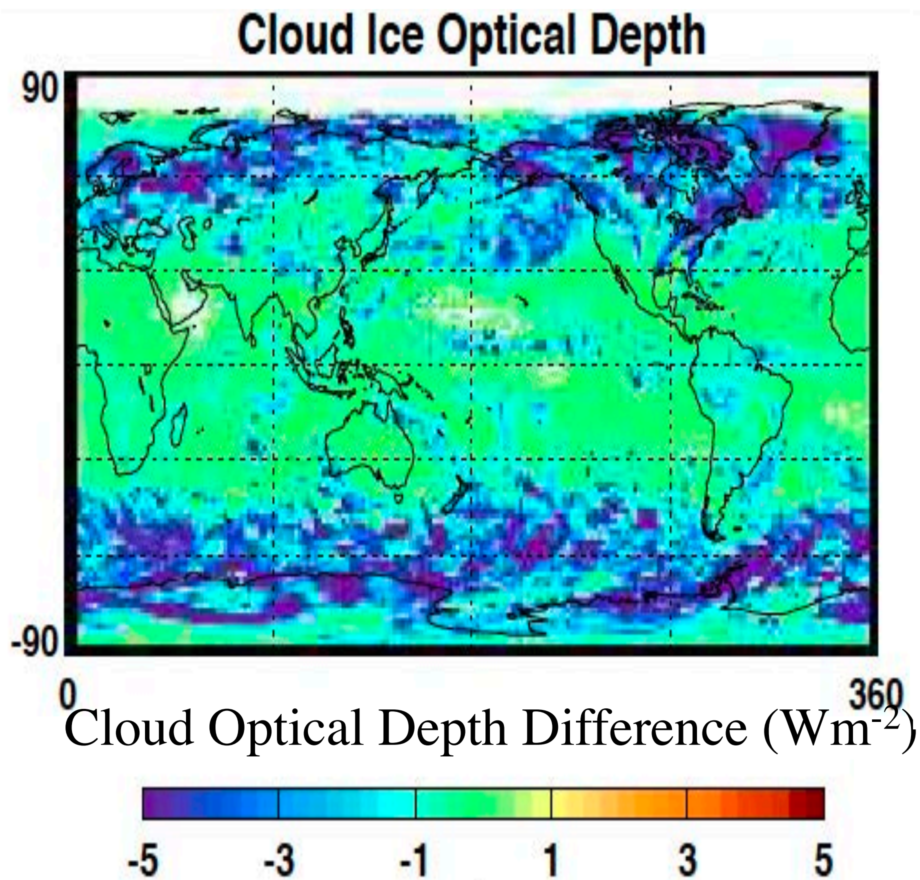

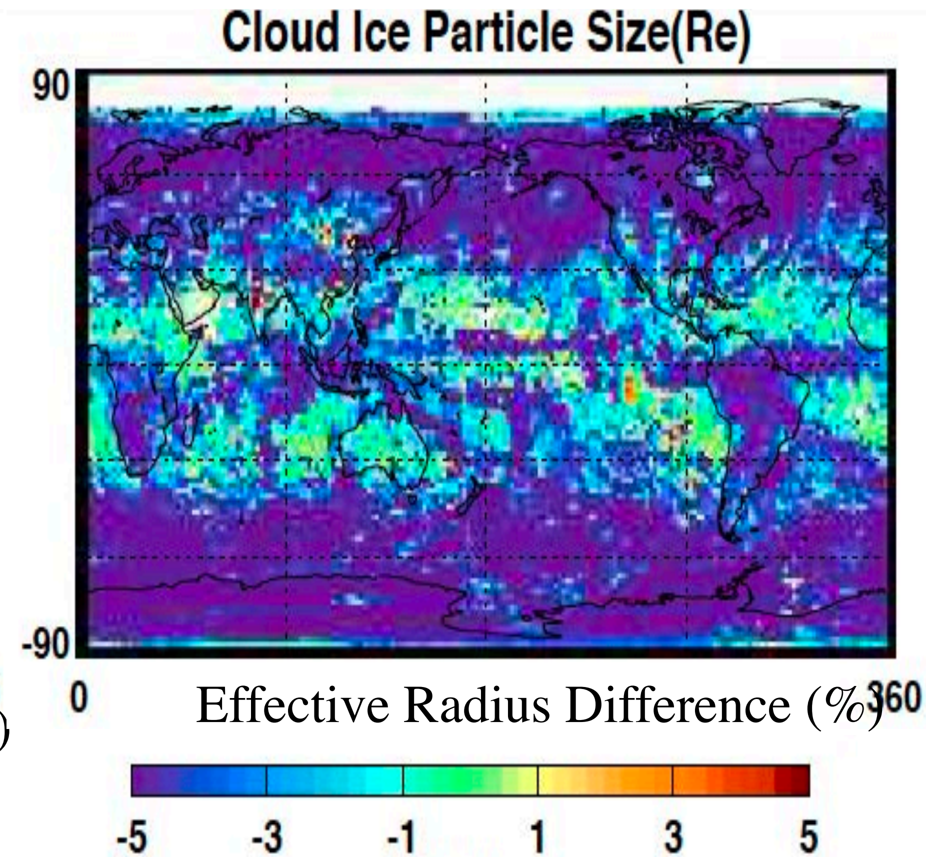

- Overall optical depth difference is -2.3 (-28% of Global Mean) and RMS difference is 2.8 (32% of GM).
- Overall effective radius difference is -3.9 ∝m (16% of GM) and RMS difference is 5.2 ∝m (16% of GM).

Loeb et al., 2018: Impact of ice microphysics on satellite cloud retrievals and broadband flux radiative transfer model calculations. *J. Climate*, 31, 1851-1864.

SW TOA Flux Difference at Aqua Overpass Time

(THM(Retriveal)/THM(Downstream) minus Smooth(Retrieval)/Smooth(Downstream))

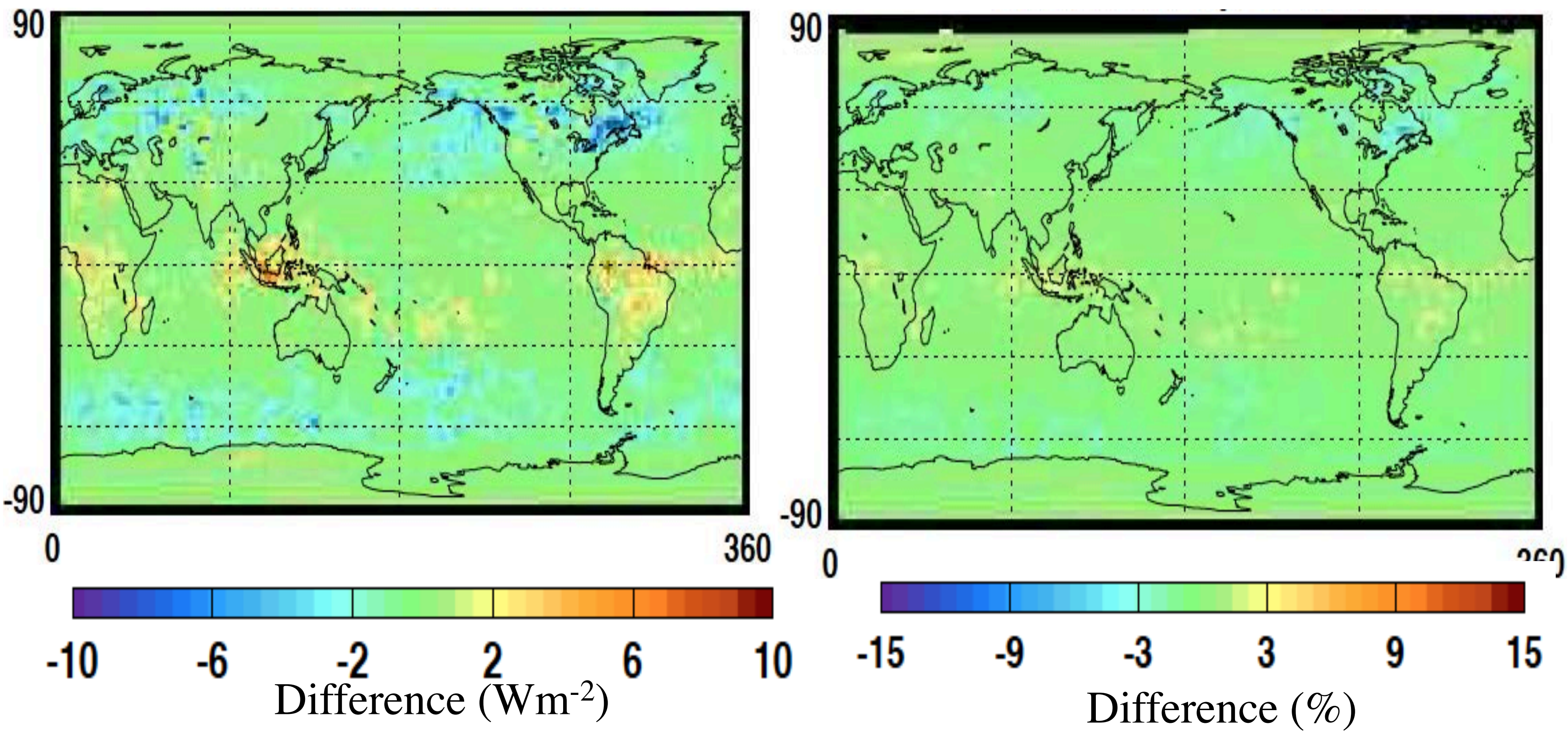

- Overall regional RMS difference is ~1%. However, in some locations regional differences reach 3%.
- Differences tend to be positive in tropics and negative in midlatitudes.

Findings by Loeb et al. (2018): radiative fluxes derived using a consistent ice particle model assumption throughout provide a more robust reference for climate model evaluation compared to existing ice cloud property retrievals.

In other words, the same ice model must be consistently used in forward remote sensing implementation (look-up tables) and downstream radiative forcing assessment.

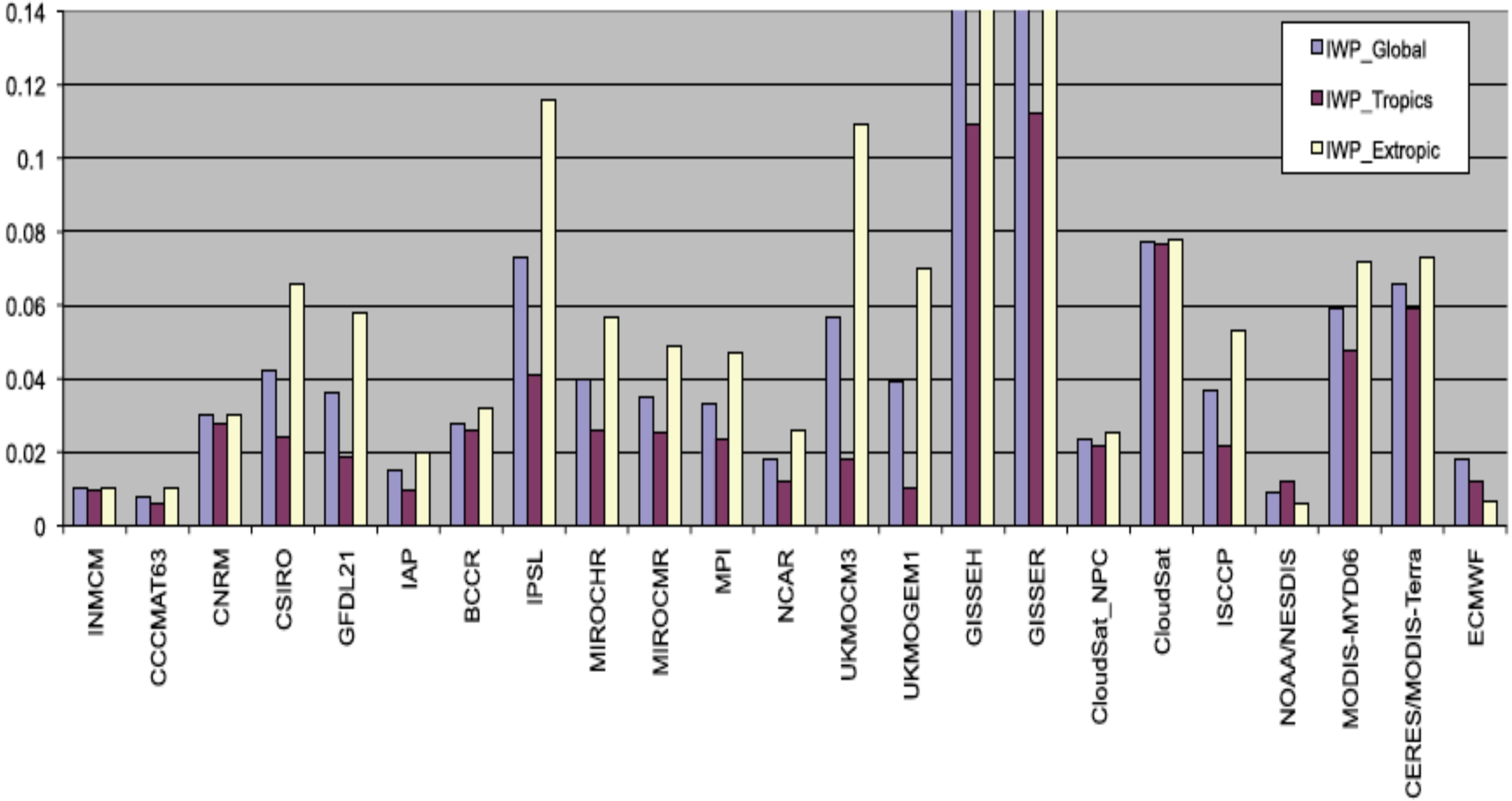

Global (blue), tropical (30° N–30° S; red) and extratropical (>30° N,S; yellow) spatial mean values of cloud ice-water path (kg m^{-2}) for 23 GCM simulations (adapted from Waliser et al., 2009). Note that the blue (yellow) bars of GISSEH and GISSER that extend above the top of the plot have values of 0.21 and 0.22 (0.34 and 0.36), respectively. Observations are shown in the

Ice Water Path (IWP),

Optical Thickness (tau)

Effective Particle size (D_{eff})

IWP = constant • tau • D_{eff}

Summary

- **Consistency hypothesis**: *radiative fluxes derived using a consistent ice particle model assumption throughout provide a more robust reference for climate model evaluation compared to existing ice cloud property retrievals* (Loeb et al. 2017). In other words, *the same ice model must be consistently used in forward remote sensing implementations and downstream radiative transfer computations*.

- **Objectives**

1) Validate the consistency hypothesis by using the MODIS, AIRS, and CALIPSO cloud property products, CERES flux products, and state-of-the-science light scattering and radiative transfer modeling capabilities in conjunction with the ice cloud models used by the respective science teams.
2) Quantify the global scale uncertainties/errors caused by using inconsistent ice cloud models
3) **Develop parameterization schemes** for ice cloud bulk radiative properties that are consistent with the ice models used in NASA's cloud property retrieval products